Water Research 133 (2018) 319–337

Contents lists available at ScienceDirect

Water Research

journal homepage: www.elsevier.com/locate/watres

Towards the development of a modeling framework to track nitrogen export from lowland artificial watersheds (polders)

Jiacong Huang [a, b], George B. Arhonditsis [b], Junfeng Gao [a, *], Dong-Kyun Kim [b], Feifei Dong [b]

[a] Key Laboratory of Watershed Geographic Sciences, Nanjing Institute of Geography and Limnology, Chinese Academy of Sciences, 73 East Beijing Road, Nanjing 210008, China
[b] Ecological Modelling Laboratory, Department of Physical & Environmental Sciences, University of Toronto, Toronto, ON M1C 1A4, Canada

ARTICLE INFO

Article history:
Received 19 July 2017
Received in revised form
3 January 2018
Accepted 4 January 2018
Available online 8 January 2018

Keywords:
Polders
Nitrogen dynamics
Water budget
Best management practices
Paddy land

ABSTRACT

Excess nitrogen (N) export from lowland artificial watersheds (polders) is often assumed to be a major contributor to the cultural eutrophication of downstream aquatic ecosystems. However, the complex transport processes characterizing lowland areas pose significant challenges in accurately quantifying their actual role. In this study, we developed a dynamic model to track N sources and transport pathways in lowland polders. The model is able to accommodate all the unique characteristics of polder dynamics, including artificial drainage, and interactions among surface water, groundwater and soil water. Our model was calibrated and validated against water level data and nitrogen concentrations measured in a lowland polder (Polder Jian) in China during the 2014–2016 period. Model performance was satisfactory with an R^2 value of 0.55 and an *NS* value of 0.53 for total N concentrations. The characterization of the various components of water budget and N cycle derived by the model was on par with local empirical estimates. N export from Polder Jian was approximately 57 kg ha^{-1} yr^{-1} and was distinctly higher than values reported from nearby non-polder areas. The largest fraction of N export stemmed from seepage. To our knowledge, this is the first dynamic model to quantify N export from a watershed with artificial drainage network and can be used to design remedial measures of ecosystem degradation.

1. Introduction

Polder is a reclaimed lowland area with manual control of runoff and water levels using pumping systems (Segeren, 1983). It is widely constructed at the lowland areas of large aquatic systems around the world, such as 60% of Netherlands' land surface (van der Grift et al., 2016), the lower reach of Yangtze River (Huang et al., 2016), the upper Rhine River and Elbe River (Lindenschmidt et al., 2009). Polders functionally resemble to artificial watersheds characterized by significantly different water transport dynamics compared with free drainage watersheds. Runoff water is freely flowed through the river network within the watershed. Polders are enclosed by dikes with artificial drainage systems (e.g., culverts and pumping stations). During rainfall events, runoff water flows into the surface water area (ditches and ponds), and may be exported into surrounding rivers through culverts or pumping stations to reduce flood risk. Compared with free drainage watersheds, polders are characterized by a strong interplay among surface water, groundwater, and soil water in farmlands (Brauer et al., 2014; Yan et al., 2016). Water transport within a polder is predominantly driven by water level difference, which could result in a changing flow direction through time.

Nitrogen (N) export from lowland polders is a thorny issue due to their ability to modulate the nature and severity of eutrophication problems in adjacent aquatic ecosystems (van der Grift et al., 2016). Tracking N dynamics in polders can thus be helpful to pinpoint the major N sources to their surrounding lakes and rivers. However, the unique N transport pathways in polders pose significant challenges in accurately characterizing all the major sources and sinks of the N cycle. In particular, polder N transport is significantly affected by artificial drainage. During rainfall events, runoff water may be manually retained in the surface water area (e.g., ponds and ditches), rather than exported into their surrounding rivers (Huang et al., 2016). Such water retention within polders can profoundly change N dynamics through sedimentation and/or

* Corresponding author.
E-mail addresses: jchuang@niglas.ac.cn (J. Huang), gaojunf@niglas.ac.cn (J. Gao).

https://doi.org/10.1016/j.watres.2018.01.011
0043-1354/

other biogeochemical processes. Polder N transport is also significantly affected by strong interactions among surface water, groundwater, and soil water in farmlands.

Many process-based watershed models have been developed to simulate watershed N dynamics, such as the Soil and Water Assessment Tool (SWAT) (Arnold et al., 2012), Integrated Nitrogen in CAtchments model (INCA) (Wade et al., 2002) and Annualized Agricultural Non-Point Source Pollution (AnnAGNPS) model (Li et al., 2015). These watershed models cannot be directly applied to simulate polder N dynamics for two basic reasons. First, none of these models is structurally equipped to determine flow direction in lowland polders. One of their fundamental assumptions is that the watershed is spatially divided into hydrologic response units (HRUs) or grid cells, whereby flow direction is determined based on elevation differences among these HRUs/cells. However, flow direction in lowland polders is generally determined by water level rather than elevation differences. Second, the commonly-used watershed models do not include the process of artificial drainage, such as culvert and pumping stations, although there is ample evidence in the literature that they can play a significant role in N transport within polders.

In this context, our study aims to address a major knowledge gap in the modelling literature by presenting the Nitrogen Dynamic Polder (NDP) model to characterize N sources, sinks, and transport/reaction pathways. The model aims to accommodate, both conceptually and operationally, the unique processes underlying polder water balance and N transport. Our case study to illustrate the key features of the NDP model is the Polder Jian located in the lowland area of Lake Taihu Basin, China. Our analysis involves all the major methodological steps during model development, including a sensitivity analysis exercise and model optimization with genetic algorithms. Our model is then used to shed light on all the major components of the water budget and N cycle, and our derived projections are compared against existing empirical and/or modeling estimates in the area. We conclude by discussing the prospect of the model to guide management decisions as well as the potential directions for future model augmentations.

2. Model description

NDP included five water balance modules and three N dynamic modules using a daily time step. Compared with existing watershed models (e.g., SWAT), NDP includes specific mechanisms to describe water balance and N transport in lowland polders. These mechanisms considered the artificial drainage and water exchange processes among surface water, groundwater and soil water in farmlands. Mathematical equations for the processes in NDP can be found in Table A1 based on the equation numbers in Fig. 1. NDP comprises three N forms, i.e., oxidized (or nitrate/nitrite) nitrogen (*NO*), reduced nitrogen (*NH*) and particulate nitrogen (*PN*). Dissolved nitrogen (*DN*) is the sum of *NO* and *NH*. Total nitrogen (*TN*) is the sum of *NO*, *NH* and *PN*. NDP consists of 10 state variables, 31 input variables, 82 intermediate variables and 53 parameters (Tables A2 and A3). Details regarding the model implementation can be found in the Supporting Information section.

2.1. Water balance modules

Five water balance modules are used to describe the hydrological processes of polders. These modules were originally developed

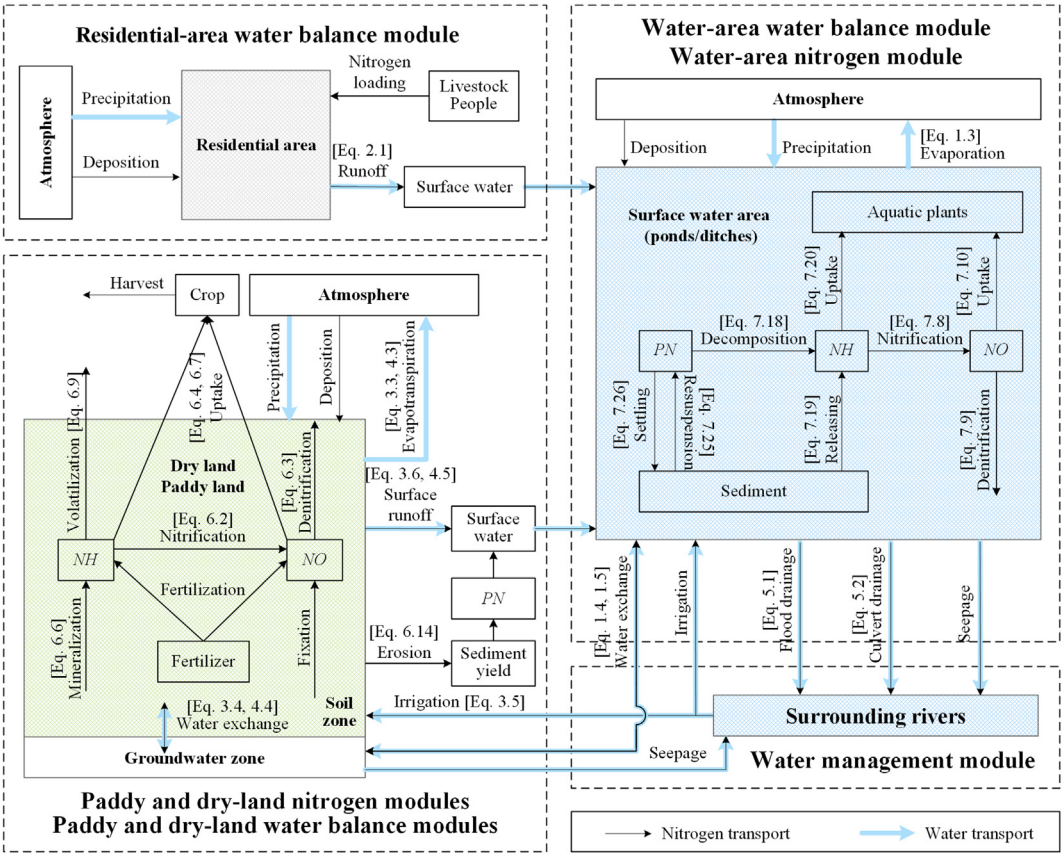

Fig. 1. Conceptual diagram for the Nitrogen Dynamic Polder (NDP) model. *NO*, oxidized nitrogen; *NH*, reduced nitrogen; *PN*, particulate nitrogen. Corresponding equations can be found in Table A1 based on the equation numbers near the arrows.

by Huang et al. (2016) in a phosphorus dynamic model for polders (PDP). Four water balance modules aim to simulate the water balance in four land-use types (residential area, surface water area, paddy and dry lands). A fifth water management module is also included aiming to describe the artificial drainage in polders, such as irrigation, culvert, and flood drainage. To better describe water balance in polders, three improvements on the water balance modules were made.

2.1.1. Interaction between groundwater and surface water

Previous studies identified a strong interaction between farmland groundwater and surface water (Brauer et al., 2014; Yan et al., 2016). The interaction resulted in quick water flow among different water layers that significantly influenced polder water balance. The interaction process was added into the water balance modules using the following exponential equation.

$$k_{Exchange} = \begin{cases} k_1 \left(\dfrac{H_{xUG}^T}{H_x^T} \right)^{\lambda_1} & H_{xUG}^T > H_x^T \\ k_2 \left(\dfrac{H_x^T}{H_{xUG}^T} \right)^{\lambda_2} & H_{xUG}^T < H_x^T \end{cases} \quad (1)$$

where $k_{Exchange}$ is the water exchange rate between farmland groundwater and surface water (m d^{-1}). H_{xUG}^T and H_x^T are the water storage (m) of the farmland groundwater and surface water. k_1 and k_2 are the maximum water exchange rate (m d^{-1}) affected by the hydraulic conductivity of soil layers. λ_1 and λ_2 are the exponential order to estimate water exchange rate. This equation describes the water exchange rate between surface water and farmland groundwater based on their water head differences, and is an application of Darcy's law (Sophocleous, 2002). A larger difference of water head would result in a larger water exchange rate (Fig. 2). Spatial variability of groundwater level was not considered.

2.1.2. Interaction between groundwater and soil water

In lowland areas, groundwater level is generally high and showed significant fluctuations over time (Cheng et al., 2006), indicative of a strong interaction between groundwater and soil water in farmlands. The water exchange rate between groundwater and soil water in paddy and dry lands is estimated using Equation (1). A higher difference between groundwater level (m) and soil water storage (m) would result in greater water exchange rate.

2.1.3. Artificial drainage

Artificial drainage (e.g., irrigation, culvert and flood drainage) was described in the water management module developed by Huang et al. (2016). The improvement of this study is the development of two approaches to describe the irrigation and pumping processes. One approach used five thresholds for water levels to describe the artificial drainage (Huang et al., 2016). This approach can be used in case that irrigation and pumping data are unavailable. More details can be found in the Supporting Information section. The second approach directly uses the measured irrigation and pumping water amount as model inputs. The present study used the latter approach as both irrigation and pumping data were available (Section 3).

2.2. Paddy and dry-land nitrogen modules

Two nitrogen modules were developed to describe the chemical and biological processes related to N dynamics in the paddy and dry lands. These nitrogen modules were developed, based on the farmland N cycle, as depicted in the Integrated Nitrogen in CAtchments (INCA) model, and soil erosion quantification, as approximated by the Universal Soil Loss Equation (USLE).

INCA is a process-based model that was originally developed by Wade et al. (2002). In this study, it was selected due to its detailed mechanisms for describing *NO* and *NH* dynamics in the soil zone of agricultural farmlands (Lazar et al., 2010; Wade et al., 2006; Whitehead et al., 2016). *NO* concentrations in soil water are determined by fertilization, deposition, atmospheric nitrogen (N_2) fixation, nitrification, denitrification and crop uptake. *NH* concentrations in soil water are driven by fertilization, deposition, mineralization (organic N to *NH*), nitrification and crop uptake. *NO* and *NH* dynamics in the soil water of the dry and paddy lands can be described using the following equations.

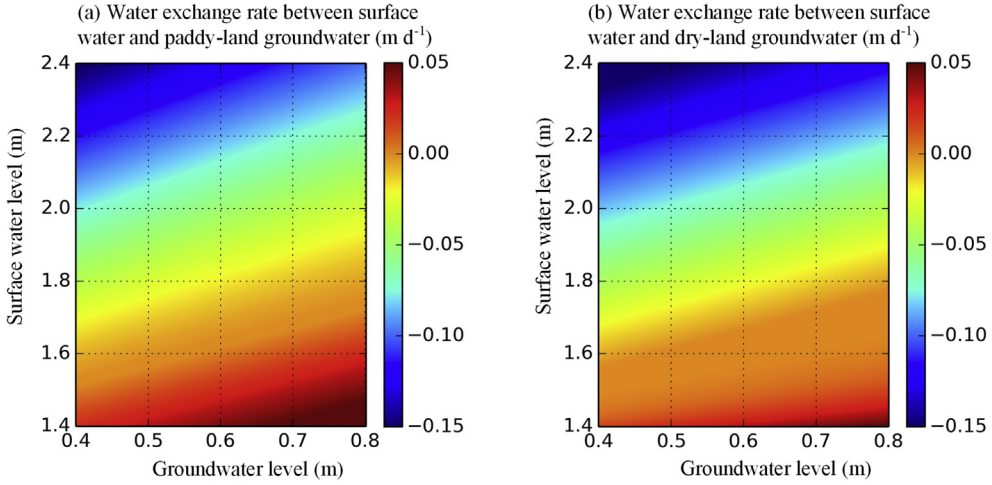

Fig. 2. Water exchange rate between surface water and groundwater in paddy (a) and dry lands (b). Positive value represents water flow from surface water to paddy and dry-land groundwater. Negative value represents water flow from paddy and dry-land groundwater to surface water. The figure was drawn based on Equation (1) and the potential ranges of groundwater level and surface water level.

$$NO_x^T = \frac{NO_x^{T-\Delta T} H_x^{T-\Delta T} + \Delta NO_{xFert}^T + \Delta NO_{xDep}^T}{H_x^T} + \frac{0.1 k_{xNOFix} + \Delta NH_{xNit}^T - \Delta NO_{xDenit}^T - \Delta NO_{xUptake}^T}{H_x^T} \quad (2)$$

$$NH_x^T = \frac{NH_x^{T-\Delta T} H_x^{T-\Delta T} + \Delta NH_{xFert}^T + \Delta NH_{xDep}^T}{H_x^T} + \frac{\Delta NH_{xMine}^T - \Delta NH_{xNit}^T - \Delta NH_{xUptake}^T}{H_x^T} \quad (3)$$

where NO_x^T and NH_x^T are *NO* and *NH* concentrations in the soil water of the dry and paddy lands at time *T*. H_x^T is soil water storage of the dry and paddy lands at time *T*. ΔNO_{xFert}^T and ΔNH_{xFert}^T are mass change of *NO* and *NH* in the soil water of the dry and paddy lands due to fertilization at time *T*. ΔNO_{xDep}^T and ΔNH_{xDep}^T are mass change of *NO* and *NH* in the soil water of the dry and paddy lands due to dry and wet deposition at time *T*. k_{xNOFix} is N_2 fixation rate in the dry and paddy lands. ΔNH_{xNit}^T and ΔNO_{xDenit}^T are mass change of *NO* in the soil water of the dry and paddy lands due to nitrification and denitrification at time *T*. $\Delta NO_{xUptake}^T$ and $\Delta NH_{xUptake}^T$ are mass change of *NO* and *NH* in the soil water of the dry and paddy lands due to crop uptake at time *T*. ΔNH_{xMine}^T is mass change of *NH* in the soil water of the dry and paddy lands due to mineralization at time *T*.

USLE was used to estimate the annual sediment yield (kg ha^{-1} yr^{-1}) from paddy and dry lands as a function of rainfall, soil erodibility, topography, cropping and soil conservation practices (Equation 6.15 in Table A1). *PN* concentrations in the dry and paddy-land runoff were then estimated using the annual sediment yield (Equation 6.14 in Table A1). USLE was chosen because its capacity to predict soil erosion has been examined in watersheds worldwide (Kinnell, 2010), and is integrated into many watershed models, such as SWAT (Neitsch et al., 2005) and AGNPS (Young et al., 1989). Detailed description of the associated equations can be found in Neitsch et al. (2005).

2.3. Water-area nitrogen module

Polders included a large area of surface water (ponds and ditches) for retention, and therefore a water-area nitrogen module is necessary to describe N sedimentation and other biogeochemical processes in polder surface waters. The water-area nitrogen module aimed to describe N dynamics in the surface water, and was developed based on two existing aquatic models: Environmental Fluid Dynamics Code (EFDC) (Tetra Tech, 2007) and the eutrophication model for Lake Washington (Arhonditsis and Brett, 2005). The water-area nitrogen module included the processes of atmospheric deposition, nitrification, denitrification, decomposition, *PN* settling and resuspension, N release from sediments, N uptake by plants (Fig. 1). Limitations imposed by ambient temperature, *DO,* and N concentrations on nitrification, denitrification, and plant uptake were described, postulating Michaelis-Menten kinetics with half saturation constants provided by the vast body of literature available (Arhonditsis and Brett, 2005; Park et al., 2008; Tetra Tech, 2007). Compared with existing complex aquatic models, the water-area nitrogen module has two simplifications of N biogeochemical processes: (*i*) We considered only three N forms (*NO*, *NH* and *PN*), while existing lake models generally include more forms of N (e.g., five N forms in EFDC). (*ii*) We did not explicitly include a dynamic representation of the nutrient-phytoplankton interface (e.g., nutrient uptake, phytoplankton growth, basal metabolism, settling), which is generally an important component in existing lake models. These structural simplifications had the advantage of reducing input data and parameters, and were deemed defensible because this study involved polder N export rather than surface water eutrophication.

3. Model application

3.1. Study area

Polder Jian (10.6 ha) is located in the lowland area of Lake Taihu Basin, China. It is a typical lowland polder enclosed by dikes with artificial drainage and complex ditch-pond network. The main difference with free drainage watersheds is that the polder uses artificial drainage systems (one culvert and three pumping stations) for water exchange with surrounding rivers. During heavy rainfall events, the culvert and flood pumping stations (Fig. 3) are used to control surface water level to minimize flood risk. Another two pumping stations are used for irrigation during rice season. A complex ditch-pond network has been developed by local farmers for water transport and retention purposes. The ditch network transports irrigation water to agricultural farmlands for crop water requirements during the dry periods, and receives runoff from different land uses to ponds during heavy rainfall events.

The polder has a diversity of land-use types including paddy land (50.1%), dry land (21.7%), residential areas (19.2%), and surface water (9%). The paddy land has a double-cropping system of rice in summer and wheat in winter. Inorganic fertilizers, including urea (46.4% N) and compound fertilizers (16% N and 16% P), has been used for crops in dry and paddy lands. Organic fertilizers are scarcely used for crops.

3.2. Data collection

To investigate the polder nutrient dynamics, an intensive monitoring program has been conducted since 2014 within the study area (Polder Jian). Based on the monitoring program, a three-year (2014–2016) dataset was collected to calibrate and validate the NDP model. This dataset included land use, fertilization rates, meteorological, hydrological and water quality data with their detailed information in Table 1. The land use and meteorological data were used as model inputs, while the hydrological and water quality data were mainly used for model calibration and validation.

The land use data were based on satellite images. The fertilization data were collected from local farmers. The meteorological data were measured using an automatic rain gauge (HOBO RG3-M) at Polder Jian and the national weather station (Liyang) near the polder. The hydrological data included water level, irrigation, and flood drainage. Water level data were collected during 2015–2016 using a water level logger (HOBO U20) at Polder Jian. There were several data gaps in 2015 due to some instability issues with the water level logger. Irrigation and flood drainage data were derived based on the recorded pumping time. All the meteorological and hydrological data were averaged to a daily time scale. The water quality data were collected by water and sediment sampling at W1-4 and S1-3 (Fig. 3), respectively.

3.3. Model calibration and validation

NDP included two parameter sets consisting of 28 parameters for the water balance modules and 25 parameters for the N dynamic modules. These two parameter sets were sequentially calibrated using the time-series water level and water quality data (Table 1). The parameter set for the water balance module was calibrated and validated against the 2015 and 2016 water level data,

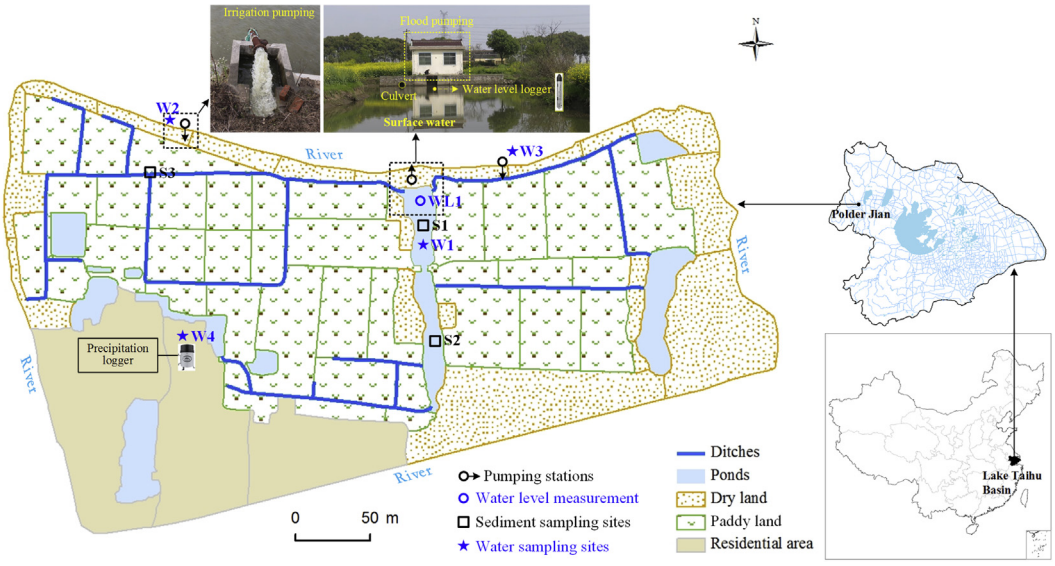

Fig. 3. The location of Polder Jian in China, descriptions of its land uses and sampling sites. Redrawn from Huang et al. (2016).

Table 1
Data collected for the Nitrogen Dynamic Polder (NDP) model.

Type	Indicator	Source	Time period	Temporal resolution	Sampling site (Fig. 3)
Land use	Land use type	Satellite image and surveying	2014–2016	–	–
Fertilization	Fertilizer amount	Survey	2014–2016	–	–
	Fertilization date				
Meteorology	T_{Max}, T_{Min}, T_{Ave}, *Wet*, *WS* and H_{Sun}	Weather station	2014–2016	Daily	Liyang
	Pr	Rain gauge	2014–2016	Hourly	W4
Hydrology	*WL*	Water level logger	2015–2016	Hourly	WL1
	Irrigation and flood drainage	Monitoring	2014–2016	Daily	W2-3
Water quality	*DN* and *PN*	Water sampling	2014–2016	Twice a month	W1-4
	TN	Sediment sampling	2014	–	S1-3

Note: T_{Max}, T_{Min} and T_{Ave}: daily maximum, minimum and average of air temperature (°C); *Wet*: daily average humidity (%); *WS*: daily average wind speed (m s^{-1}); H_{Sun}: daily sunshine hours (h); *Pr*: daily precipitation (mm); *WL*: water level (mm); *DN*: dissolved nitrogen concentration (mg L^{-1}); *PN*: particulate nitrogen concentration (mg L^{-1}).

respectively. The parameter set for the N dynamic module was calibrated against a two-year (2014–2015) dataset and was subsequently validated against water quality data from 2016. Model implementation in Polder Jian involved four critical steps: preliminary calibration, sensitivity analysis, model optimization, and model validation (Fig. 4). Preliminary calibration aimed to obtain an initial parameter set, resulting in an acceptable model performance, which formed the basis for the rest three methodological steps. Sensitivity analysis identified the ten most sensitive parameters for the water balance and N dynamic modules. These twenty sensitive parameters were further used for model optimization. Model validation evaluated model agreement with an independent dataset, reflecting different conditions from those used during our calibration exercise.

3.3.1. Preliminary calibration

Our goal with the preliminary model calibration was to identify a parameter vector, resulting in an acceptable model fit to the observed data, which formed the basis for the subsequent model sensitivity analysis and optimization. We used Latin Hypercube to efficiently sample the multidimensional parameter space and generate 1000 parameter vectors (Table A2). The selection of the single best parameter set was not based solely on model fit but also on the plausibility of the water and N balance budgets relative to reported ranges from previous studies within the Lake Taihu Basin (See Supporting Information section). In doing so, we ensured that each component of the water and N dynamics (e.g., farmland evapotranspiration and crop N uptake) was comparable with literature values, and thus our local sensitivity analysis was based upon a plausible base process characterization (3.3.2).

3.3.2. Sensitivity analysis

To reduce the NDP calibration parameter vector, influential parameters in the water balance and N dynamic modules were identified using a local sensitivity analysis (One-At-a-Time, OAT) method. We identified the top ten most influential parameters in the water balance and N dynamic modules using the water storage of surface water (H_{Pond}) and *TN* concentrations in surface water as the targeted variables, respectively. Each parameter value was increased or decreased by 10%, while all other parameters were kept fixed. A total of $2m$ (m is the number of the testing parameter) simulations were compared against the base simulation. The sensitivity value (S_x) of the tested parameter x was calculated by the relative change of the simulated H_{Pond} and *TN* induced by its 10% change.

$$S_x = \sum_{i=1}^{n}\left(\frac{|f_i(p_1,\ldots,p_x+\Delta,\ldots,p_m)-f_i(p_1,\ldots,p_x,\ldots,p_m)|}{2nf_i(p_1,p_2,\ldots,p_x,\ldots,p_m)\frac{\Delta}{p_x}}\right) + \sum_{i=1}^{n}\left(\frac{|f_i(p_1,\ldots,p_x-\Delta,\ldots,p_m)-f_i(p_1,\ldots,p_x,\ldots,p_m)|}{2nf_i(p_1,p_2,\ldots,p_x,\ldots,p_m)\frac{\Delta}{p_x}}\right) \quad (4)$$

where p_x is the value of the testing parameter x. $f_i(p_1,\ldots,p_x,\ldots,p_m)$

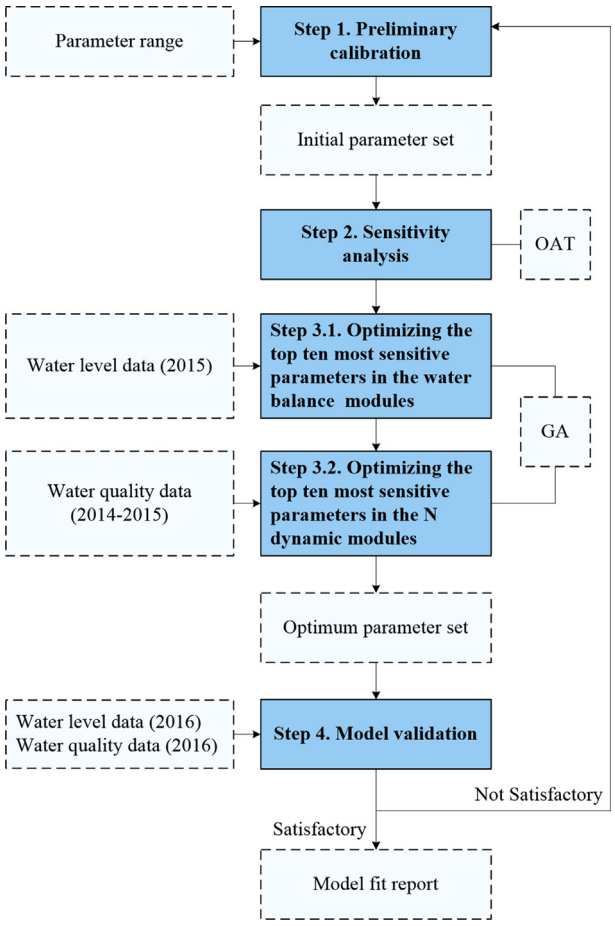

Fig. 4. Schematic illustration of model calibration and validation for the Nitrogen Dynamic Polder model. OAT, One-At-a-Time method. GA, Genetic Algorithms. N, nitrogen.

is the simulation H_{Pond} on i^{th} ($i = 1, 2, \ldots, n$) day from the base simulation. $f_i(p_1, \ldots, p_x + \Delta, \ldots, p_m)$ and $f_i(p_1, \ldots, p_x - \Delta, \ldots, p_m)$ are the simulation H_{Pond} or TN on i^{th} day from the test simulations by increasing/decreasing by Δ ($\Delta = 0.1(p_{xMax} - p_{xMin})$), respectively. p_{xMax} and p_{xMin} are the maximum and minimum values of the tested parameter x. A larger value of S_x implies a higher sensitivity of parameter x. Further implementation details of the OAT method could be found in Cariboni et al. (2007).

3.3.3. Parameter optimization using genetic algorithms

Genetic Algorithms (GA), originally proposed by Goldberg (1989), are increasingly used in environmental modeling practice for parameter estimation due to their ability to achieve global optimization (Kim et al., 2007; Liu et al., 2007). Following our sensitivity analysis exercise, two parameter sets (top ten influential parameters in water balance and N dynamic modules) were subsequently optimized using GA with water level and water quality data (Table 1). GA optimization of each parameter set required the following steps.

1. Population initialization. 200 initial parameter sets (population) were generated for the first generation of GA runs. In each parameter set, parameter values were randomly generated within their literature-based ranges (See Supporting Information section).

2. Fitness evaluation. During the training period, the fitness (F) of each individual was evaluated based upon the corresponding coefficient of determination (R^2) and Nash-Sutcliffe efficiency (NS) values.

$$F = R^2 + NS \quad (5)$$

An individual with a higher F value implied a higher fitness. R^2 is expressed as the squared ratio between the covariance and the multiplied standard deviations of the observed and simulated values. As such, it estimates the combined dispersion against the single dispersion of the observed and simulated series. However, the fact that only the dispersion is quantified is one of the major drawbacks of R^2, as a model that systematically over- or under-predicts will still result in good R^2 values (Krause et al., 2005). On the other hand, NS is defined as one minus the sum of the absolute squared differences between predicted and observed values normalized by the variance of the observed values during the period under investigation. Although a popular goodness-of-fit measure in hydrology that accounts for linear bias of the model examined, the Nash-Sutcliffe efficiency is prone to overestimate model performance with large values (e.g., peak flows) in a time series, whereas the impact of lower values (e.g., low flow conditions) tends to be downplayed (Legates and McCabe, 1999). Additional insights into the model fitness function values against parameter variations along with the covariance patterns of the two measures of fit (R^2 versus NS) are provided in the Supporting Information section.

3. Reproduction. Reproduction aiming to select the individuals with higher fitness values to create the next generation. An individual with a higher fitness (F) value, i.e., higher R^2 and NS value, had a higher chance for reproduction. Thus, the overall model fit of the individuals would be gradually improved over the course of 100 generations.

4. Crossover and mutation. For each generation, crossover was used to generate new individuals by exchanging parameter values. 80% of the individuals were used in the crossover processes. Mutation was a randomly induced change of an individual's parameter value(s) with a low probability (5%). Both crossover and mutation processes were expected to generate dissimilar individuals (parameter sets) with high model fit.

5. Optimization. Repeat steps 2–4 until the generation number reached its maximum value of 100. The individual with highest fitness in the 100th generation was the best parameter set in this run.

6. Repeated run. Repeat steps 1–5 for 100 times. The best parameter set from these 100 runs was compared to evaluate the GA's stability.

7. Mass balance evaluation. The plausibility of the characterization of the water cycle and N budget was evaluated by comparing the associated fluxes with literature reported values. This step aimed to settle for a calibration parameter set that effectively balances between optimal model performance and realistic representation of the water cycle and N dynamics in Polder Jian.

3.3.4. Calibration and validation results

Identification of the top ten most influential parameters in the water balance modules and the N dynamic modules can be found in the Supporting Information section. The calibrated parameters are given in Table A2. The water balance modules in NDP were well calibrated with an R^2 value of 0.75 and an NS value of 0.73. During the validation period (2016), the model captured the general water level trends. Several peak values were also closely reproduced. However, model fit during the validation period declined relative to that derived from model calibration (Fig. 5). The inferior performance was due to the occurrence of several extremely high/low values (e.g., Jul. 21, 2016 and Sep. 27, 2016) that were not well predicted. There were also instances of over-estimated water level

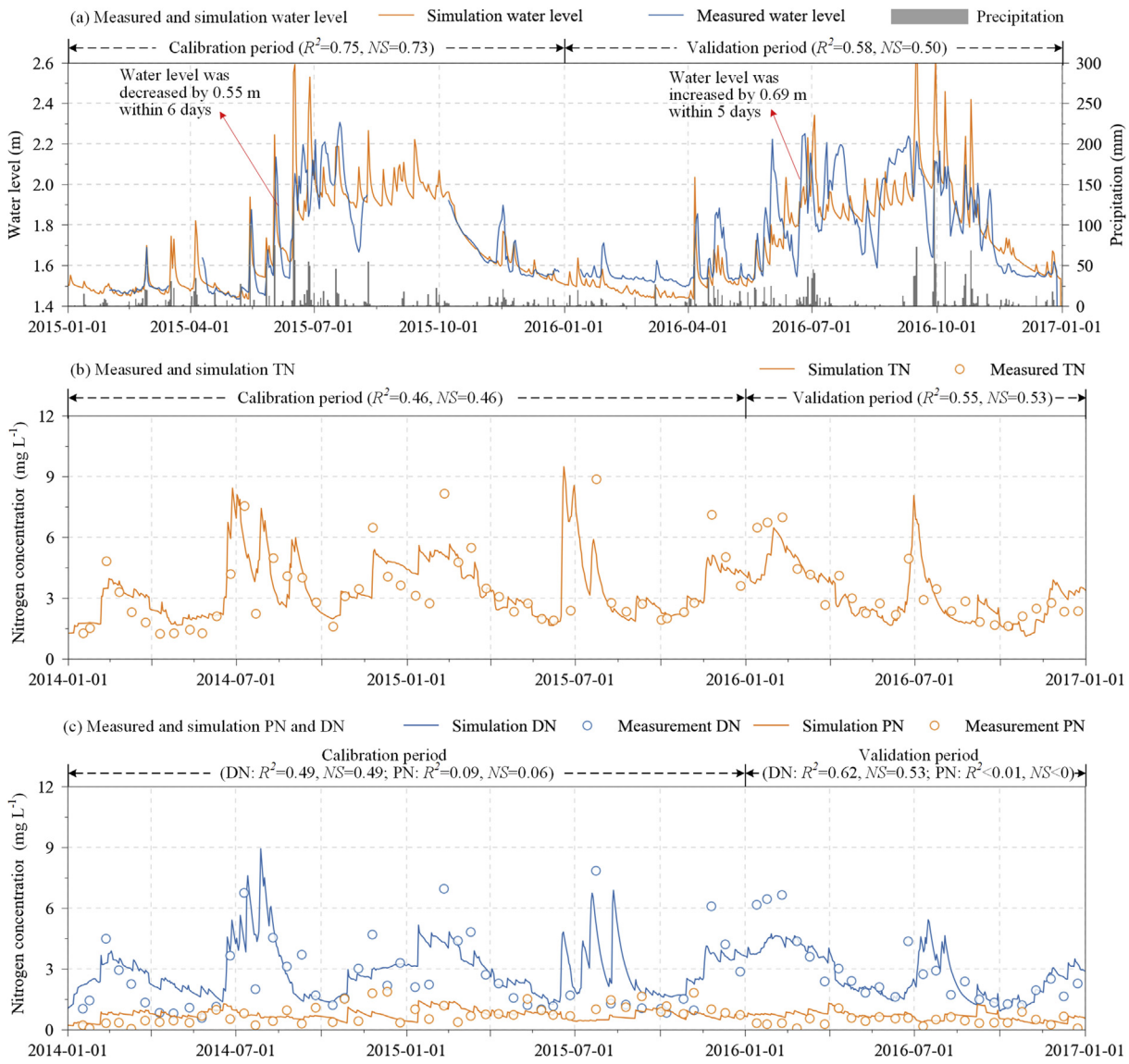

Fig. 5. Simulated and measured water level and nitrogen concentrations at station W1 during the calibration and validation domain of the NDP model. *DN*, dissolved nitrogen; *PN*, particulate nitrogen. *TN*, total nitrogen.

peaks during both calibrated and validation periods.

During the calibrated period, *TN* in surface waters was accurately simulated with an R^2 value of 0.46 and the resulting *NS* value of 0.46. Measured *TN* showed a decreasing trend from February to June, and an increasing trend from October to December. These trends were also closely reproduced by the model (Fig. 5). Interestingly, model fit for *TN* concentrations during the validation period was slightly better than that for the calibration period. The NDP model also accounted for *DN* and *PN* dynamics in the polder (Fig. 5c). The agreement between simulated and measured *DN* data was slightly better than with the *TN* data, whereas *PN* was characterized by higher discrepancies which also reflected in an *NS* value less than 0.1 during the calibration and validation periods.

3.4. Water balance

In Polder Jian, the main water sources were precipitation and irrigation. Precipitation mainly occurred in summer and autumn (Fig. 5), and showed a large year-to-year variability ranging from 1376.8 to 1506.5 mm yr^{-1}. The annual precipitation in 2016 (1506.5 mm) was the highest over the past twenty years (1996–2015) with an average annual precipitation of 1139.9 mm. The annual irrigation was 536.0 mm for the polder, i.e., 1069.8 mm yr^{-1} for paddy land. In previous studies of double-cropping (rice and wheat) farmlands in Lake Taihu Basin, Xu et al. (2012) reported an irrigation rate of 878 mm yr^{-1}, while Zhao et al. (2012) reported an irrigation level of 507.9–572.6 mm yr^{-1} without considering the water loss through ditches during irrigation period. The large use of irrigation water for the polder was mainly due to the large water surface area (9% of Polder Jian) and low elevation of dry land that caused a disproportionally high movement of irrigation water downstream.

The water in Polder Jian is lost through surface water evaporation, farmland evapotranspiration, seepage, culvert, and flood drainage (Fig. 6). The annual farmland evapotranspiration was 491.5 mm for the polder or 679.2 mm yr^{-1} for paddy and dry lands. This estimate was very close to reported value (632 mm yr^{-1}) from an experimental study in Lake Taihu Basin (Xu et al., 2012). Flood drainage had a value of 118.3 mm yr^{-1}, and mostly occurred during extreme precipitation period. As shown in Fig. 6, flood drainage was

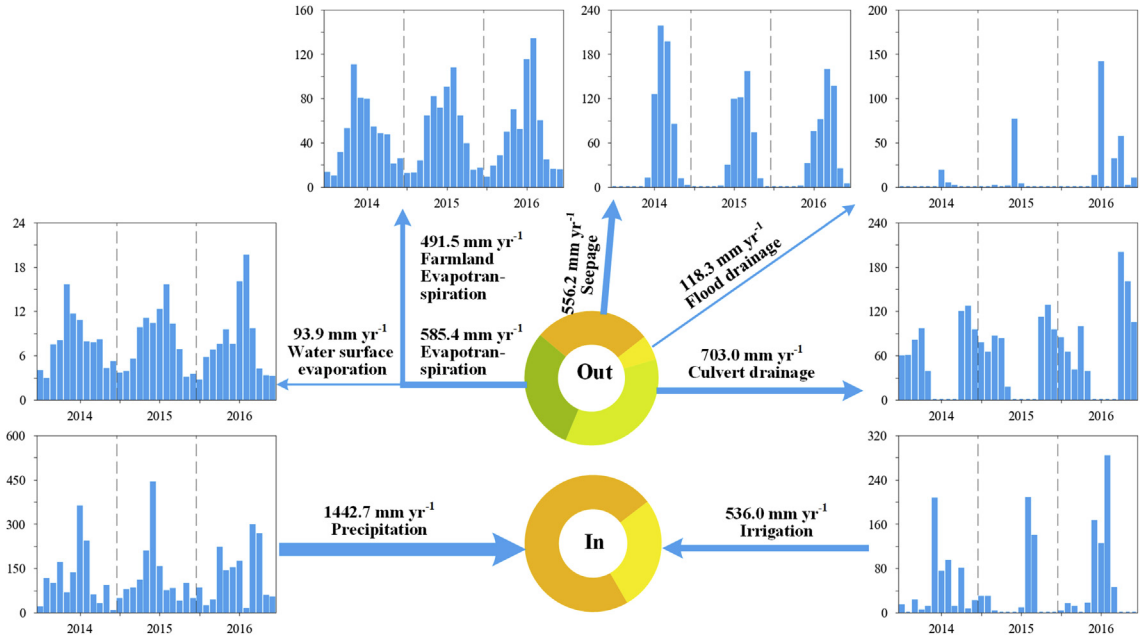

Fig. 6. Characterization of the water cycle in Polder Jian, as derived from the daily simulation results during 2014–2016. In, water inputs into the polder. Out, water outputs from the polder. Monthly dynamics of water balance components are represented using bar graph. All water balance components are derived based on the polder area.

high (251.4 mm) in 2016 due to several extreme precipitation events. Culvert drainage and seepage were responsible for a large proportion of water export out of Polder Jian with values of 703.0 and 556.2 mm yr^{-1}, respectively. Culvert was closed during the rice season and thus the associated drainage occurred only during the rest of the year. Seepage had a large value in the summer mainly due to the large water level differences between surface water and surrounding rivers (Fig. 5).

3.5. Nitrogen balance

Our modeling analysis showed that fertilization and mineralization were the major N sources for Polder Jian (Fig. 7). Fertilization contributed 73.3% (450 kg ha^{-1} yr^{-1}) of total N sources to the polder. The inter-annual variability was negligible based on the survey from local farmers over the course of the study. Mineralization had an estimated contribution of 116.1 kg ha^{-1} yr^{-1} for agricultural farmlands. This estimate lies within the reported range from previous studies in Lake Taihu Basin (Table 2). Deposition, irrigation, and N_2 fixation represented a small fraction (<8.0%) of N input in the polder. It is also worth noting that although irrigation is a major source of water (Fig. 6), its contribution as N source appears to be fairly low (<2.0%).

The major N sinks for Polder Jian were crop uptake, volatilization, and denitrification (Fig. 7). Crop N uptake was the largest N sink with an estimated value of 365.6 kg ha^{-1} yr^{-1}. Previous studies provided evidence of large variability associated with crop N uptake rate ranging from 246 to 375 kg ha^{-1} yr^{-1} in Lake Taihu Basin (Table 2). Volatilization and denitrification had an estimated rate of 117.7 and 89.7 kg ha^{-1} yr^{-1}. Seepage mostly occurred in summer, and had an N export rate of 40.6 kg ha^{-1} yr^{-1}. Culvert and flood drainage accounted for a small proportion (<5%) of total N sinks.

From a management perspective, N export into surrounding rivers is a critical facet of the polder functioning that could be used to determine the appropriate remedial measures for alleviating the eutrophication severity downstream. Based on the N balance in Polder Jian, N export rates from Polder Jian were estimated by subtracting N import through irrigation from the sum of N export through seepage, culvert and flood drainage. The resulting value could be used as a proxy for the polder N contribution to surrounding rivers. Our estimated N export coefficient (56.7 kg ha^{-1} yr^{-1}) in Polder Jian was distinctly higher than N export coefficients (6.0–20.4 kg ha^{-1} yr^{-1}) reported for Lake Taihu Basin from past studies (Lai et al., 2006; Li et al., 2015; see also Table 2). Seepage was characterized by a larger N export than surface discharge (culvert and flood drainage). Polder N export mainly occurred in the summer and displayed greater year-to-year variability.

4. Discussion

Despite decades of research on nutrient export dynamics from watersheds, non-point sources of excess nutrients continue to be primarily responsible for the impairment of the quality of receiving water bodies. The recognition of this problem invites the development of watershed models that can support water quality management goals, such as the estimation of non-point source nutrient loads and the examination of alternative land use scenarios. Nonetheless, the field of process-based, distributed watershed modeling is dominated by a handful of models (SWAT, INCA, AGNPS/AnnAGNPS, HSPF, and HBV), which have fairly similar representations of spatial variability, relevant flow paths, and nutrient biogeochemistry (Wellen et al., 2015). It is thus argued that existing model structures fail to accommodate contemporary ideas of observational hydrology/biogeochemistry, and have an unproven ability to reproduce the complex interplay among hydrological factors, morphological features, and mechanisms that modulate nutrient and contaminant attenuation rates in artificial watersheds (e.g., polders). Being subjected to significantly different water transport dynamics compared with free drainage systems, the latter issue provided the motivation for the application of our N dynamic model in the Polder Jian in Lake Taihu Basin, China.

4.1. Model performance

The key augmentations of our dynamic model involved the representation of artificial drainage, as well as the water

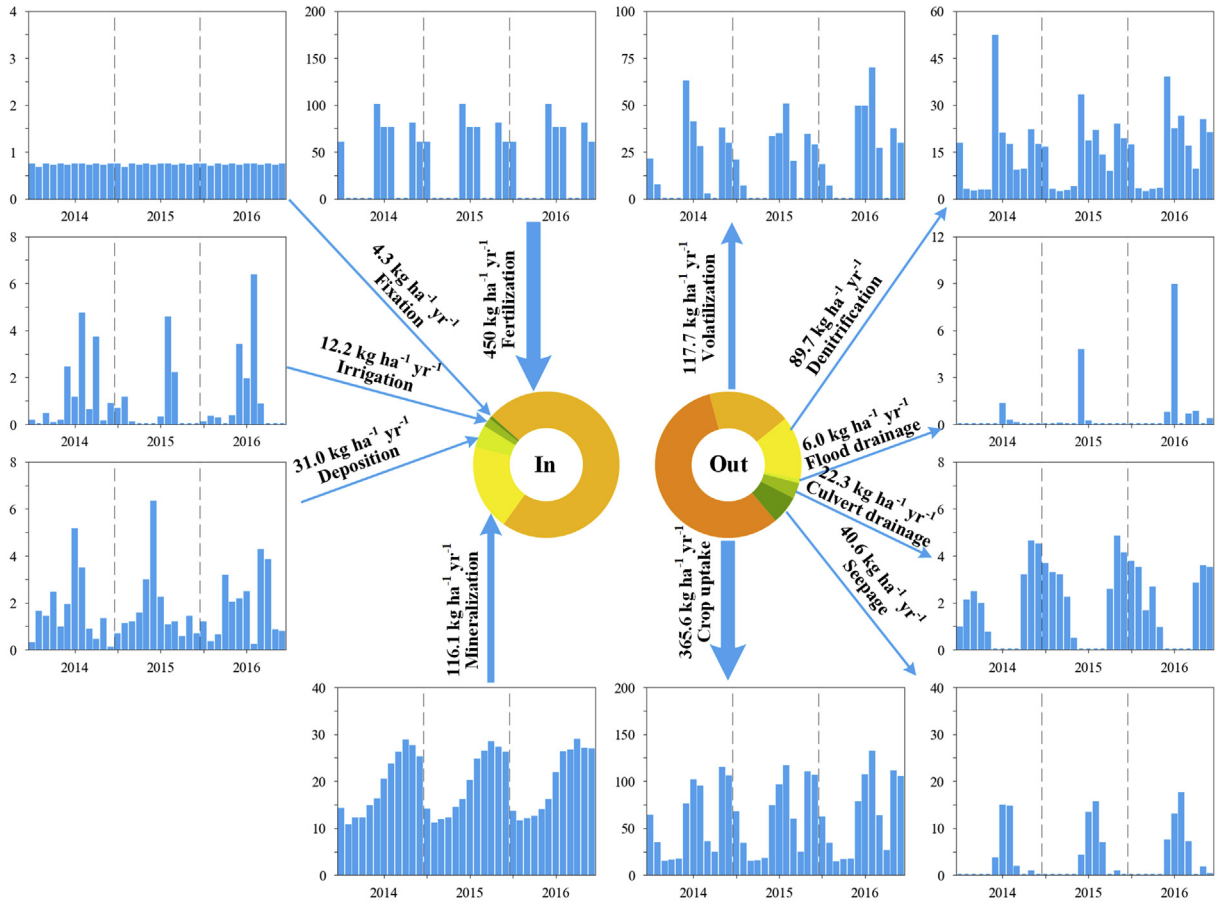

Fig. 7. Characterization of the nitrogen cycle in Polder Jian, as derived from the daily simulation results during 2014–2016. In, nitrogen inputs into the polder. Out, nitrogen outputs from the polder. Monthly dynamics of nitrogen balance components are represented using bar graph. Seepage, culvert and flood drainage were derived based on the polder area, other components of the nitrogen cycle are derived based on the paddy and dry-land area.

interactions among surface water, groundwater, and soil water in farmlands (Section 2.1). These two mechanisms were particularly important due to their significant impact on polder water balance and our results rendered support to our strategy (Fig. 5). In particular, the water level was decreased by 0.55 m within 6 days during June 3–8, 2015, suggestive of flood pumping and/or water exchange between surface water and other layers of water (i.e., groundwater and soil water). On the other hand, although no major rainfall events had occurred, the water level was increased by 0.69 m within 5 days during June 20–24, 2016, which likely stemmed from artificial irrigation.

We implemented standard methodological steps (i.e., sensitivity analysis, parameter optimization, and validation) during the application of our model in order to identify the most influential parameters, to maximize model fit to the calibration dataset, and to examine its reliability in drawing predictions in the extrapolation domain (Arhonditsis and Brett, 2004). Nonetheless, this methodological consistency does not appear to be the norm in the contemporary watershed modeling practice. For example, based on a sample of 257 watershed models published in the peer-reviewed literature, Wellen et al. (2015) found that 57% of the studies conducted model validation, while only 17% implemented parameter optimization. Compared with these 257 surveyed models, the *NS* value of our *TN* simulations (0.53) was indicative of model performance that is better than more than half of the published body of watershed modeling work (Wellen et al., 2015). We also found that *DN* matched closely the observed data relative to *PN*. *PN* was not well predicted especially during the validation period (Fig. 5). We hypothesize that the limited capacity of our model to capture the *PN* concentrations stems from the highly dynamic nature of the settling-minus-resuspension processes and consequently the inherent unpredictability of their net effect on the particulate matter in the surface waters of Polder Jian. However, the inferior model performance with *PN* concentrations is not particularly troublesome in this study, because *DN* accounted for 80% of the ambient *TN* levels. Thus, the satisfactory model fit to *TN* predominantly reflects its ability in predicting *DN*. Counter to many previous studies that evaluated model reliability only on the basis of model fit to observed data, our study explicitly recognized the fact that complex overparameterized models can give "good results" for the "wrong reasons" (Arhonditsis et al., 2007), and we thus evaluated the plausibility of the water and N cycle characterization in Polder Jian (see Sections 3.4 and 3.5). The values of critical processes (e.g., irrigation and fertilization) assigned during our model calibration were comparable with estimates reported from previous studies in Lake Taihu Basin (Table 2; see also following section).

In a similar manner, our model performance was also on par with the results presented by previous N modeling work within the Lake Taihu Basin. An earlier study by Lai et al. (2006) used the SWAT model to provide preliminary estimates of N export from the entire Lake Taihu Basin, and reported model fit with R^2 values varying from 0.40 to 0.85 and *NS* values within the 0.53–0.78 range. Zhao et al. (2011b) simulated *TN* loading from six monitoring sites in the Xitiaoxi catchment in Lake Taihu Basin using a PCRaster-based

Table 2
Comparison of the quantitative estimates of various components of the water and nitrogen cycles in Polder Jian with previous studies within Lake Taihu Basin.

Process	Polder Jian	Previous studies within Lake Taihu Basin
Water balance components (mm yr^{-1})		
Irrigation	1069.8	878 (Xu et al., 2012)
		507.9–572.6 (Zhao et al., 2012)
Farmland evapotranspiration	679.2	632 (Xu et al., 2012)
Nitrogen balance components for farmlands (kg ha^{-1} yr^{-1})		
Fertilization	450	510 (Qiao et al., 2012)
		465-635 (Richter and Roelcke, 2000)
		452 (Hofmeier et al., 2015)
		425-635 (Zhao et al., 2011b)
		500 (Zhao et al., 2012)
		550 (Zhao et al., 2009)
		394-569 (Zhang et al., 2013)
N_2 Fixation	4.3	13 (Hofmeier et al., 2015)
		4.3 (Zhao et al., 2011b)
Irrigation	12.2	12 (Hofmeier et al., 2015)
		10.0–14.4 (Zhao et al., 2012)
Deposition	31.0	9.0–19.5 (Richter and Roelcke, 2000)
		28 (Hofmeier et al., 2015)
		9.2–11.5 (Zhao et al., 2011b)
		30.5 (Zhao et al., 2012)
Mineralization	116.1	165 (Zhang et al., 2013)
		74–167.3 (Zhao et al., 2011b)
Crop uptake	365.6	311.5 (Zhang et al., 2013)
		257-320 (Richter and Roelcke, 2000)
		358 (Hofmeier et al., 2015)
		246-375 (Zhao et al., 2011b)
		263-304 (Zhao et al., 2012)
		341.7 (Zhao et al., 2009)
Denitrification	89.7	18.4–39.6 (Zhao et al., 2011b)
		121.9–144 (Zhao et al., 2012)
Volatilization	117.7	71.5–147.9 (Zhao et al., 2012)
		>125.27 (Xu et al., 2012)
		>103.56 (Liang et al., 2007)
Seepage	40.6	12.4–65.6 (Zhao et al., 2011b)
Nitrogen export coefficient (kg ha^{-1} yr^{-1})		
Nitrogen export	56.7	6.0–6.7 (Li et al., 2015)
		20.4 (Lai et al., 2006)

model of nutrient mobilization and transport, founded upon the integration of the Xinanjiang rainfall-runoff model with the Integrated Nitrogen CAtchment model and the Modified Universal Soil Loss Equation. The model displayed satisfactory agreement to the *TN* concentrations at the downstream sites with a *NS* range of 0.38–0.59 and a R^2 range of 0.52–0.62, although the measured data were characterized by a broader range (0.5–5.2 mg L^{-1}) relative to the upstream locations. Interestingly, model performance declined at the latter sites with a *NS* range of 0.25–0.27 and a R^2 range of 0.42–0.54. The same analysis indicated that the fertilizer implementation (425–635 kg N ha^{-1} yr^{-1}) and the atmospheric deposition (22–25.8 kg N ha^{-1} yr^{-1}) were the dominant N input processes, whereas N removal from the catchment was mainly attributed to plant uptake, ammonium volatilization, denitrification, and leaching through runoff.

4.2. Polder nitrogen sources and sinks: implications for management

During the past decade, a significant body of literature has attempted to establish causal linkages between severe algal blooms in Lake Taihu and nutrient loading from the surrounding watershed (Huang et al., 2012; Qin et al., 2010). The simulated results of Polder Jian using NDP revealed that fertilization and bacteria-mediated mineralization were the major N sources, whereas crop uptake, volatilization and denitrification were the major N sinks (Fig. 7). N fertilizer implementation in farmlands in Polder Jian was 450 kg ha^{-1} yr^{-1} during 2014–2016. N plant uptake rate demonstrated substantial variability, ranging from 246 to 375 kg ha^{-1} yr^{-1} (Table 2). After the harvest, when grain and chaff have been removed, the dry stalks of cereal plants partly remain within the farmlands, where they are subjected to mineralization and replenish the soil N pool available for crop uptake. N volatilization mostly occurs after fertilization with a particularly high rate, when conditions of low soil water, high air temperature, wind speed, and radiation prevail (Xu et al., 2012). Although volatilization does not directly pose threats to the adjacent water bodies, increased N emissions are likely to elevate the atmospheric concentrations, which in turn could conceivably lead to enhanced N deposition in the long-run (Liu et al., 2013). Conversion of nitrate into N_2 via denitrification is another major N sink pathway from the Polder Jian and typically occurs under flooded water conditions (Wang et al., 2017).

By comparing the characterization of N cycle relative to reports of previous studies in Lake Taihu Basin (Table 2), two unique patterns of N dynamics were found in this study.

- Annual N export (56.7 kg ha^{-1} yr^{-1}) in the Polder Jian was higher than existing estimates (6.0–20.4 kg ha^{-1} yr^{-1}) from the rest of the Lake Taihu Basin (Table 2). The elevated polder N export likely accentuates the severity of eutrophication in the downstream waterbodies, and can be attributed to large farmland areas and intensive farming with excessive N fertilizer application (Hofmeier et al., 2015). Interestingly, N fertilizer application rates in Polder Jian ($\approx$450 kg ha^{-1} yr^{-1}) were at the lower end of those typically reported in Lake Taihu Basin during

the 1990s (465–635 kg ha^{-1} yr^{-1}; see Richter and Roelcke (2000)). In the same context, it is also worth noting that a recent study by Hofmeier et al. (2015) argued in favour of a reduction in N fertilizer application rates by 15–25% for summer rice and by 20–25% for winter wheat without significant decrease in mean grain yields.

- Seepage had the largest N export among the major pathways (seepage, culvert and flood drainage) from the studied polder system. The high seepage rate in Polder Jian was probably due to the large water level differences between polder surface water and the streams surrounding the system. This pattern was particularly pronounced during the dry summer period, when polder surface water levels were fairly high due to irrigation and stream water levels reached their seasonal minima. The high seepage rate also implied that N removal from polder surface water is critical for mitigating excessive N export.

4.3. Potential uses of the Nitrogen Dynamic Polder model

Compared with existing watershed models, our NDP model effectively described the processes underlying water balance and N fate and transport in lowland areas with artificial drainage, and can thus be used in other lowland polders with strong interactions among surface water, groundwater, and soil water. After the characterization of the water budget and N cycle, including the quantitative description of the relationship between polder N balance and environmental conditions (e.g., weather, irrigation, and fertilization conditions), the model can be used to answer important management questions, such as "*What is a realistic reduction target of polder N export, given the increasing demand for a higher crop production from an ever-growing population?*", "*What are the best management practices to mitigate N export, based on the current characterization of the water and N cycles in Polder Jian?*" or "*How effective can these remedial measures be, given the presence of an active nutrient regeneration feedback loop in the polder?*" Such investigation will not only help water managers to identify the important factors controlling polder N export, but can also assist with the design of the optimal management strategies for protecting our precious water resources.

To implement NDP in a new case study, model users can simply specify their input data based on the template prepared for the case study in Polder Jian, China. Sensitivity analysis, calibration, and validation for the new case study are strongly encouraged in order to establish a reliable modelling tool that can effectively guide environmental management. Sensitivity analysis will allow identifying the most sensitive parameters for the new case, while model calibration and validation based on time-series data collected from the targeted polder are critical for obtaining an optimal parameter set and ideally achieving a defensible process characterization (Arhonditsis and Brett, 2004).

4.4. Model uncertainty

In the context of model-based environmental management, there are several compelling reasons to rigorously quantify model uncertainty and effectively communicate the robustness of predictive statements in policy analysis frameworks (Arhonditsis et al., 2007). N balance analysis (Section 3.5) showed that fertilization, mineralization, crop uptake, volatilization and denitrification were the main N sources and sinks for Polder Jian. Interestingly, a post-hoc exercise revealed that fertilization and crop uptake contribute more to the overall model uncertainty relative to the rest of the processes considered (Section 5.1. in Supporting Information). This result provides evidence of the importance to further improve our estimates of fertilization rates in the studied basin as well as to design field experimentation that will causally connect crop uptake rates with soil characteristics (e.g., texture, porosity, organic matter or nutrient content) and weather conditions typically prevailing in the area.

We also conducted another post-hoc exercise to connect the model fitness function F with the variations in the values of the twenty most influential parameters (Section 5.2. in Supporting Information). The corresponding panels in Fig. SI-5 offer proxies of the marginal parameter distributions and their fairly uninformative (flat) patterns are reflective of the well-known equifinality (poor model identifiability) problem, where several distinct choices of model inputs lead to the same model outputs (many sets of parameters fit the data about equally well) (Beven, 2006). A main reason for the equifinality problem is that the ecological processes/causal mechanisms used for understanding how the system works internally is of substantially higher order than what can be externally observed. In fact, our exercise was able to narrow down the behavioural range, associated with acceptable model performance, for only three parameters, i.e., maximum water storage of the surface water controlled by the culver ($H^{Max}_{Culvert}$), maximum water export rate through culvert ($k^{Max}_{Culvert}$), coefficient of temperature influence on the processes related to N dynamics in the dry and paddy lands (θ_x).

A thorough uncertainty analysis was so far not implemented, as is the case with the majority of the studies presenting complex over-parameterized models, like NDP, that tend to overlook the issue of equifinality. Instead, they usually strive for the identification of a global optimum in the parameter space that will maximize model fit to the observed data. Reflecting the popular stance that any scientific endeavour should aspire to achieve a single correct description of the reality, issues related to model parametric uncertainty or even to the adequacy of a model structure are typically downplayed (Beven, 2006). Although the present analysis was conceptually consistent with the latter practice, we must emphasize that our optimization exercise identified multiple local optima and led to moderate model fit improvement after 100 generations (see Fig. SI-3 in our Supporting Information section). To overcome this problem, we opted for an examination of the plausibility of the water and N cycle specifications, as depicted by the optimum calibration vector, but the credibility of the model in guiding management decisions about future investments to the environment can be significant leveraged by conducting a more comprehensive uncertainty analysis. To this end, recognizing that complex models may not be easily subjected to uncertainty analysis, there is a growing field of research aiming to develop methods that effectively overcome their large computational demands (e.g., advanced numerical methods, adaptive Markov chain Monte Carlo techniques, statistical emulators), thereby enabling rigorous uncertainty assessment on even the most complex environmental models (Castelletti et al., 2012; Kim et al., 2014; Reichert et al., 2011).

5. Conclusions

We presented the NDP model specifically designed to characterize N sources, sinks, and transport/reaction pathways in lowland artificial watersheds (polders). The model was applied to a typical lowland polder (Polder Jian) in China, and achieved a satisfactory model fit along with a realistic characterization of the water budget and N cycle. Our modeling exercise revealed that polders have higher N export potential than non-polder areas and seepage may

have the largest contribution among the pathways considered in our model. Our study highlighted the significant impact of artificial drainage practices on water balance, which are manually controlled and thus can be easily recorded. For example, the culvert is generally closed during the rice season to keep the water inside the polder, but culvert managers may export some water out of the polder to minimize the risk of flooding before a heavy rainfall event. A systematic record of such external interventions will be beneficial for our model, as these knowledge gaps may rectify some of the discrepancies between empirical and simulated patterns reported in our study. Human disturbances, such as land use changes and aquatic plant harvest at ditches, can also significantly influence polder N dynamics. Improving our understanding of the impact of these processes will also bolster the predictive capacity of our model by reducing both structural and parametric uncertainty. Conceptually, the present modeling exercise draw parallels with viewpoints that render support to the use of complex over-parameterized models, even though their structure could be an impediment for rigorous and complete error analysis. Complex models offer excellent heuristic tools allowing insights into the direct, indirect, and synergistic effects of a multitude of ecological mechanisms that form the foundation of system behaviour. The Nitrogen Dynamic Polder model can be particularly useful in this direction.

Acknowledgments

We would like to thank editor and reviewers for their helpful comments. The project was financially supported by Natural Science Foundation of Jiangsu, China (BK20161614), Water Resources Science and Technology Program of Jiangsu, China (2017040) and National Natural Science Foundation of China (41301574). The authors would like to thank China Meteorological Data Sharing Service System for providing the measured data for model development. Special thanks to China Scholarship Council for providing fellowship to visit University of Toronto, Canada. Special thanks to Prof. Michael Rode (Helmholtz Centre for Environmental Research, Germany) for his help on model development, and to Cindy Yang (University of Toronto, Canada) for insightful comments on an earlier version of the manuscript.

Appendix A. Supplementary data

Supplementary data related to this article can be found at https://doi.org/10.1016/j.watres.2018.01.011.

Appendix A

Table A1
Main equations of the Nitrogen Dynamic Polder (NDP) model.

No.	Equation	Description and reference
1	**Water-area water balance module**	
1.1	$H_{Pond}^{T} = H_{Pond}^{T-\Delta T} + \Delta H_{Pond}^{T} + H_{PondIrr}^{T} - H_{Pump}^{T} - H_{Culvert}^{T}$	Water level dynamics
1.2	$\Delta H_{Pond}^{T} = Pr^{T} + \frac{H_{TownQ}^{T} S_{Town}}{S_{Pond}} + \frac{H_{PaddyQ}^{T} S_{Paddy}}{S_{Pond}} + \frac{H_{DryQ}^{T} S_{Dry}}{S_{Pond}} - E_{Pond}^{T} - H_{PondSeep}^{T} + H_{PondPaddyUGExchange}^{T} + H_{PondDryUGExchange}^{T}$	Water balance
1.3	$E_{Pond}^{T} = \frac{f_{Penman}(T_{Ave}^{T}, T_{Max}^{T}, T_{Min}^{T}, Wet^{T}, H_{Sun}^{T}, WS^{T}, Pr^{T}, P_{Ave}^{T}, Lat)}{\alpha_{Ev}}$	Surface water evaporation (Chen et al., 2005)
1.4	$H_{PondPaddyUGExchange}^{T} = \begin{cases} -f_{exp}(H_{Pond}^{T}, H_{PaddyUG}^{T})^{\lambda_{Pond2PaddyUG}} & H_{Pond}^{T} > H_{PaddyUG}^{T} \\ f_{exp}(H_{Pond}^{T}, H_{PaddyUG}^{T})^{\lambda_{PaddyUG2Pond}} & H_{Pond}^{T} < H_{PaddyUG}^{T} \end{cases}$	Water exchange between paddy-land groundwater and surface water
1.5	$H_{PondDryUGExchange}^{T} = \begin{cases} -f_{exp}(H_{Pond}^{T}, H_{DryUG}^{T})^{\lambda_{Pond2DryUG}} & H_{Pond}^{T} > H_{DryUG}^{T} \\ f_{exp}(H_{Pond}^{T}, H_{DryUG}^{T})^{\lambda_{DryUG2Pond}} & H_{Pond}^{T} < H_{DryUG}^{T} \end{cases}$	Water exchange between dry-land groundwater and surface water
1.6	$H_{PondSeep}^{T} = k_{PondSeepMax} f_{exp}(H_{Pond}^{T})^{\lambda_{PondSeep}}$	Water seepage in the surface water
2	**Residential-area water balance module**	
2.1	$H_{TownQ}^{T} = \begin{cases} rc_{Town} Pr^{T} & Pr_{Cum}^{T} \geq H_{TownFill} \\ 0 & Pr_{Cum}^{T} < H_{TownFill} \end{cases}$	Residential-area runoff (Rossi et al., 2004; Taebi and Droste, 2004)
3	**Paddy-land water balance module**	
3.1	$H_{Paddy}^{T} = H_{Paddy}^{T-\Delta T} + \Delta H_{Paddy}^{T} + H_{PaddyIrr}^{T} - H_{PaddyQ}^{T}$	Soil water balance in paddy land
3.2	$\Delta H_{Paddy}^{T} = Pr^{T} - E_{Paddy}^{T} + H_{PaddyUGExchange}^{T}$	Water balance
3.3	$E_{Paddy}^{T} = kc_{Paddy}^{T} f_{Penman}(T_{Ave}^{T}, T_{Max}^{T}, T_{Min}^{T}, Wet^{T}, H_{Sun}^{T}, WS^{T}, Pr^{T}, P_{Ave}^{T}, Lat)$	Paddy-land evapotranspiration (Allen et al., 1998; Cai et al., 2007)
3.4	$H_{PaddyUGExchange}^{T} = \begin{cases} -k_{PaddyInfMax} f_{exp}(H_{Paddy}^{T}, H_{PaddyUG}^{T}) & H_{Paddy}^{T-\Delta T} + Pr^{T} - E_{Paddy}^{T} \geq H_{Paddy}^{Sat} \\ k_{PaddyCapMax} f_{exp}(H_{Paddy}^{T}, H_{PaddyUG}^{T}) & H_{Paddy}^{T-\Delta T} + Pr^{T} - E_{Paddy}^{T} < H_{Paddy}^{Sat} \end{cases}$	Water exchange between groundwater and soil water in paddy land (Li et al., 2014)
3.5	$H_{PaddyIrr}^{T} = \frac{\alpha_{Irr} V_{Irr}^{T}}{S_{Paddy}}$	Paddy-land irrigation
3.6	$H_{PaddyQ}^{T} = \begin{cases} (H_{Paddy}^{T-\Delta T} + \Delta H_{Paddy}^{T}) - H_{Paddy}^{Flood} & H_{Paddy}^{T-\Delta T} + \Delta H_{Paddy}^{T} \geq H_{Paddy}^{Flood} \\ 0 & H_{Paddy}^{T-\Delta T} + \Delta H_{Paddy}^{T} < H_{Paddy}^{Flood} \end{cases}$	Paddy-land runoff (Huang et al., 2016)
3.7	$H_{PaddyUG}^{T} = H_{PaddyUG}^{T-\Delta T} - H_{PaddyUGExchange}^{T} - H_{PondPaddyUGExchange}^{T} - k_{UGSeepMax} f_{exp}(H_{PaddyUG}^{T})^{\lambda_{PaddyUGSeep}}$	Water balance
4	**Dry-land water balance module**	
4.1	$H_{Dry}^{T} = H_{Dry}^{T-\Delta T} + \Delta H_{Dry}^{T} - H_{DryQ}^{T}$	Soil water balance in dry land
4.2	$\Delta H_{Dry}^{T} = Pr^{T} - E_{Dry}^{T} + H_{DryUGExchange}^{T}$	Water balance
4.3	$E_{Dry}^{T} = kc_{Dry}^{T} f_{Penman}(T_{Ave}^{T}, T_{Max}^{T}, T_{Min}^{T}, Wet^{T}, H_{Sun}^{T}, WS^{T}, Pr^{T}, P_{Ave}^{T}, Lat)$	Dry-land evapotranspiration (Allen et al., 1998; Cai et al., 2007)
4.4	$H_{DryUGExchange}^{T} = \begin{cases} -k_{DryInfMax} f_{exp}(H_{Dry}^{T}, H_{DryUG}^{T}) & H_{Dry}^{T-\Delta T} + Pr^{T} - E_{Dry}^{T} \geq H_{Dry}^{Sat} \\ k_{DryCapMax} f_{exp}(H_{Dry}^{T}, H_{DryUG}^{T}) & H_{Dry}^{T-\Delta T} + Pr^{T} - E_{Dry}^{T} < H_{Dry}^{Sat} \end{cases}$	Water exchange between groundwater and soil water in dry land (Chen and Liu, 2002)

Table A1 (*continued*)

No.	Equation	Description and reference
4.5	$H_{DryQ}^{T}=\begin{cases} H_{Dry}^{T-\Delta T}+\Delta H_{Dry}^{T}-H_{Dry}^{Flood} & H_{Dry}^{T-\Delta T}+\Delta H_{Dry}^{T}\geq H_{Dry}^{Flood} \\ 0 & H_{Dry}^{T-\Delta T}+\Delta H_{Dry}^{T}<H_{Dry}^{Flood} \end{cases}$	Dry-land runoff (Huang et al., 2016)
4.6	$H_{DryUG}^{T}=H_{DryUG}^{T-\Delta T}-H_{DryUGExchange}^{T}-H_{PondDryUGExchange}^{T}-k_{UGSeepMax}f_{\exp}(H_{DryUG}^{T})^{\lambda_{DryUGSeep}}$	Water balance
5	**Water management module**	
5.1	$H_{Pump}^{T}=\frac{V_{Pump}^{T}}{S_{Pond}}$	Flood drainage
5.2	$H_{PondIrr}^{T}=\frac{(1-\alpha_{Irr})V_{Irr}^{T}}{S_{Pond}}$	Irrigation
5.3	$H_{Culvert}^{T}=\begin{cases} k_{Culvert}^{Max}\left(\frac{H_{Pond}^{T-\Delta T}+\Delta H_{Pond}^{T}-H_{Culvert}^{Max}}{H_{Culvert}^{Max}}\right)^{\lambda_{Culvert}} & Wheat\ \ season \\ 0 & Rice\ \ season \end{cases}$	Culvert drainage (Huang et al., 2016)
6	**Paddy and dry-land nitrogen modules**	
6.1	$NO_{x}^{T}=\frac{NO_{x}^{T-\Delta T}H_{x}^{T-\Delta T}+NO_{River}^{T}H_{xIrr}^{T}+0.1NO_{xFert}^{T}+\Delta NO_{xDep}^{T}+0.1k_{xNOFix}+\Delta NH_{xNit}^{T}-\Delta NO_{xDenit}^{T}-\Delta NO_{xUptake}^{T}}{H_{x}^{T}}(x\in[Paddy,Dry])$	*NO* dynamics in soil water
6.2	$\Delta NH_{xNit}^{T}=k_{xNHNit}f_{xT}f_{xW}NH_{x}^{T}H_{x}^{T}$	Nitrification (Wade et al., 2002)
6.3	$\Delta NO_{xDenit}^{T}=k_{xNODenit}f_{xT}f_{xW}NO_{x}^{T}H_{x}^{T}$	Denitrification (Wade et al., 2002)
6.4	$\Delta NO_{xUptake}^{T}=0.1k_{xNOUptake}f_{xT}f_{xW}f_{xS}$	*NO* uptake by crops (Wade et al., 2002)
6.5	$NH_{x}^{T}=\frac{NH_{x}^{T-\Delta T}H_{x}^{T-\Delta T}+NH_{River}^{T}H_{xIrr}^{T}+0.1NH_{xFert}^{T}+\Delta NH_{xDep}^{T}+\Delta NH_{xMine}^{T}-\Delta NH_{xNit}^{T}-\Delta NH_{xVola}^{T}-\Delta NH_{xUptake}^{T}}{H_{x}^{T}}(x\in[Paddy,Dry])$	*NH* dynamics in soil water
6.6	$\Delta NH_{xMine}^{T}=0.1k_{xNHMine}f_{xT}f_{xW}$	Mineralization (Wade et al., 2002)
6.7	$\Delta NH_{xUptake}^{T}=0.1k_{xNHUptake}f_{xT}f_{xW}f_{xS}$	*NH* uptake by crops (Wade et al., 2002)
6.9	$\Delta NH_{xVola}^{T}=k_{xNHVola}f_{xT}f_{xW}NH_{x}^{T}H_{x}^{T}$	*NH* volatilization
6.10	$f_{xT}=(\theta_{x})^{(T_{Soil}^{T}-20)}$	Temperature limitation (Wade et al., 2002)
6.11	$T_{Soil}^{T}=T_{Ave}^{T}-T_{MaxMin}\sin\left(\frac{3\pi d}{2\times365}\right)$	Soil water estimation (Wade et al., 2002)
6.12	$f_{xW}=\frac{H_{Def}^{Max}-H_{Def}}{H_{Def}^{Max}}$	Soil moisture limitation (Wade et al., 2002)
6.13	$f_{xS}=0.66+0.34\sin\left(2\pi\frac{d-d_{G}}{365}\right)$	Seasonal plant growth influence (Wade et al., 2002)
6.14	$PN_{Runoff}=f(TN_{Soil},Sed)$	Farmland runoff
6.15	$Sed=R_{USLE}K_{USLE}L_{USLE}S_{USLE}C_{USLE}P_{USLE}$	Soil erosion (Kinnell, 2010)
7	**Water-area nitrogen module**	
7.1	$\Delta TN_{Polder}^{T}=\Delta TN_{Pump}^{T}+\Delta TN_{Culvert}^{T}+\Delta TN_{Inf}^{T}-\Delta TN_{Irr}^{T}-\Delta TN_{Dep}^{T}$	N balance
7.2	$\Delta TN_{Irr}^{T}=10^{-3}TN_{River}^{T}V_{Irr}^{T}$	N import due to irrigation
7.3	$\Delta TN_{Dep}^{T}=(10^{-3}Pr^{T}(PN_{Pr}^{T}+NH_{Pr}^{T}+NO_{Pr}^{T})+0.1k_{DryDep})S_{Polder}$	N deposition
7.4	$\Delta TN_{Pump}^{T}=10^{-3}H_{Pump}^{T}S_{Pond}TN_{Pond}^{T}$	N export due to flood drainage
7.5	$\Delta TN_{Culvert}^{T}=10^{-3}H_{Culvert}^{T}S_{Pond}TN_{Pond}^{T}$	N export due to culvert drainage
7.6	$\Delta TN_{Seep}^{T}=10^{-3}(H_{PondSeep}^{T}S_{Pond}TN_{Pond}^{T}+H_{PaddyUGExchange}^{T}S_{Paddy}TN_{Paddy}^{T}+H_{DryUGExchange}^{T}S_{Dry}TN_{Dry}^{T})$	N export due to seepage
7.7	$NO_{Pond}^{T}=\frac{NO_{Pond}^{T-\Delta T}H_{Pond}^{T-\Delta T}+NO_{River}^{T}H_{PondIrr}^{T}+\Delta NO_{PondDep}^{T}}{H_{Pond}^{T}}+\Delta NH_{PondNit}^{T}-\Delta NO_{PondDenit}^{T}-\Delta NO_{PondUptake}^{T}+\frac{NO_{DryQ}^{T}H_{DryQ}^{T}S_{Dry}+NO_{PaddyQ}^{T}H_{PaddyQ}^{T}S_{Paddy}+NO_{TownQ}^{T}H_{TownQ}^{T}S_{Town}}{H_{Pond}^{T}S_{Pond}}$	*NO* dynamics in the surface water
7.8	$\Delta NH_{PondNit}^{T}=k_{PondNHNit}f_{PondT}f_{DONit}f_{NHNit}NH_{Pond}^{T}$	Nitrification (Arhonditsis and Brett, 2005; Omlin et al., 2001; Tetra Tech, 2007)
7.9	$\Delta NO_{PondDenit}^{T}=k_{PondNODenit}f_{PondT}f_{DODenit}f_{NODenit}NO_{Pond}^{T}$	Denitrification (Arhonditsis and Brett, 2005; Tetra Tech, 2007)
7.10	$\Delta NO_{PondUptake}^{T}=k_{PondNOUptake}f_{NOUptake}f_{Season}NO_{Pond}^{T}$	*NO* uptake by aquatic plant (Hu et al., 2006)
7.11	$f_{PondT}=e^{(-\theta^{Pond}(T_{Water}^{T}-20)^{2})}$	Temperature limitation (Arhonditsis and Brett, 2005)
7.12	$f_{DONit}=\frac{DO_{Pond}^{T}}{KH_{DONit}+DO_{Pond}^{T}}$	*DO* limitation for nitrification (Tetra Tech, 2007)
7.13	$f_{NHNit}=\frac{NH_{Pond}^{T}}{KH_{NHNit}+NH_{Pond}^{T}}$	*NH* limitation for nitrification (Tetra Tech, 2007)
7.14	$f_{DODenit}=\frac{KH_{DODenit}}{KH_{DODenit}+DO_{Pond}^{T}}$	*DO* limitation for denitrification (Tetra Tech, 2007)
7.15	$f_{NODenit}=\frac{NO_{Pond}^{T}}{KH_{NODenit}+NO_{Pond}^{T}}$	*NO* limitation for denitrification (Tetra Tech, 2007)
7.16	$f_{NOUptake}=\frac{NO_{Pond}^{T}}{KH_{NOUptake}+NO_{Pond}^{T}}$	*NO* limitation for plant uptake (Tetra Tech, 2007)
7.17	$NH_{Pond}^{T}=\frac{NH_{Pond}^{T-\Delta T}H_{Pond}^{T-\Delta T}+NH_{River}^{T}H_{PondIrr}^{T}+\Delta NH_{PondDep}^{T}+\Delta NH_{PondRele}^{T}}{H_{Pond}^{T}}+\Delta PN_{PondDecom}^{T}-\Delta NH_{PondNit}^{T}-\Delta NH_{PondUptake}^{T}+\frac{NH_{DryQ}^{T}H_{DryQ}^{T}S_{Dry}+NH_{PaddyQ}^{T}H_{PaddyQ}^{T}S_{Paddy}+NH_{TownQ}^{T}H_{TownQ}^{T}S_{Town}}{H_{Pond}^{T}S_{Pond}}$	*NH* dynamics in the surface water
7.18	$\Delta PN_{PondDecom}^{T}=k_{PondPNDecom}f_{PondT}f_{DODecom}PN_{Pond}^{T}$	Decomposition (Hu et al., 2006)
7.19	$\Delta NH_{PondRele}^{T}=k_{PondSedRele}TN_{PondSed}$	*NH* releasing from sediment

(*continued on next page*)

Table A1 (*continued*)

No.	Equation	Description and reference
7.20	$\Delta NH^T_{PondUptake} = k_{PondNHUptake} f_{NHUptake} f_{Season} NH^T_{Pond}$	*NH* uptake by aquatic plant (Hu et al., 2006)
7.21	$f_{DODecom} = \frac{DO^T_{Pond}}{KH_{DODecom} + DO^T_{Pond}}$	*DO* limitation for decomposition (Tetra Tech, 2007)
7.22	$f_{NHUptake} = \frac{NH^T_{Pond}}{KH_{NHUptake} + NH^T_{Pond}}$	*NH* limitation for plant uptake (Tetra Tech, 2007)
7.23	$f_{Season} = \frac{T^T_{Ave} - T_{AveMin}}{T_{MaxMin}}$	Seasonal change of aquatic plant
7.24	$PN^T_{Pond} = \frac{PN^{T-\Delta T}_{Pond} H^{T-\Delta T}_{Pond} + PN^T_{River} H^T_{PondIrr} + \Delta PN^T_{PondDep}}{H^T_{Pond}} - \Delta PN^T_{PondDecom} + \Delta PN^T_{PondResu} - \Delta PN^T_{PondSettling} + \frac{PN^T_{DryQ} H^T_{DryQ} S_{Dry} + PN^T_{PaddyQ} H^T_{PaddyQ} S_{Paddy} + PN^T_{TownQ} H^T_{TownQ} S_{Town}}{H^T_{Pond} S_{Pond}}$	*PN* dynamics in the surface water
7.25	$\Delta PN^T_{PondResu} = \frac{k_{PondPNResu} f_{Season}}{H^T_{Pond}}$	*PN* resuspension
7.26	$\Delta PN^T_{PondSettling} = \frac{k_{PondPNSettling}}{H^T_{Pond}} PN^T_{Pond}$	*PN* settling

Note: *DO*, dissolved oxygen; *NO*, nitrate/nitrite nitrogen; *NH*, reduced nitrogen; *PN*, particulate nitrogen; *TN*, total nitrogen (*TN* = *NO* + *NH* + *PN*); N, nitrogen.

Table A2
Parameters of the Nitrogen Dynamic Polder (NDP) model and their initial values for the case study in Polder Jian.

Symbol	Parameter	Value	Unit	Values from previous references
Parameters in the water-area water balance module				
α_{Ev}	Ratio between reference evapotranspiration and surface water evaporation	0.572		0.4–0.8 (Chen et al., 2005)
$k_{PondSeepMax}$	Maximum seepage rate of the surface water area	0.0004	m d^{-1}	
$\lambda_{PondSeep}$	Exponential order for seepage in the surface water area	0.17		
$\lambda_{Pond2DryUG}$	Exponential order for water transport from surface water to dry-land groundwater	0.013		
$\lambda_{DryUG2Pond}$	Exponential order for water transport from dry-land groundwater to surface water	0.085		
$\lambda_{Pond2PaddyUG}$	Exponential order for water transport from surface water to paddy-land groundwater	0.218		
$\lambda_{PaddyUG2Pond}$	Exponential order for water transport from surface water to dry-land groundwater	0.624		
Parameters in the residential-area water balance module				
rc_{Town}	Runoff coefficient for the residential area	0.685		0.75 (Rossi et al., 2004) 0.40–0.93 (Barrett et al., 1998) 0.55 (Taebi and Droste, 2004)
$H_{TownFill}$	Water fill amount of the residential area	0.002	m	0.002–0.01 (Cheng et al., 2006)
Parameters in the paddy-land water balance module				
$k_{PaddyInfMax}$	Maximum infiltration rate of the paddy land	0.005	m d^{-1}	0.003–0.007 (Li et al., 2014)
$k_{PaddyCapMax}$	Maximum capillary rise rate of the paddy land	0.006	m d^{-1}	
H^{Sat}_{Paddy}	Saturated soil water of the paddy land	0.120	m	0.08–0.17 (Zhao et al., 2011a)
H^{Flood}_{Paddy}	Maximum water storage of the paddy land	0.158	m	
$H^T_{PaddyMax}$	Upper limit of appropriate water storage for the paddy land	0.13 –0.17	m	0.12–0.16 (Cheng et al., 2006)
$H^T_{PaddyMin}$	Lower limit of appropriate water storage for the paddy land	0.10 –0.11	m	0.12–0.14 (Cheng et al., 2006)
kc^T_{Paddy}	Crop factor of the paddy land	0.5–1.4		0.9–1.2 (Liang et al., 2014) 1.0–1.5 (Cheng et al., 2006) 0.38–1.42 (Liu et al., 2002)
$k_{UGSeepMax}$	Maximum seepage rate of the paddy and dry-land groundwater	0.0088	m d^{-1}	
$\lambda_{PaddyUGSeep}$	Exponential order for seepage in the paddy-land groundwater	2.989		
Parameters in the dry-land water balance module				
$k_{DryInfMax}$	Maximum infiltration rate of the dry land	0.003	m d^{-1}	
$k_{DryCapMax}$	Maximum capillary rise rate of the dry land	0.004	m d^{-1}	
H^{Sat}_{Dry}	Saturated soil water of the dry land	0.088	m	0.08–0.17 (Zhao et al., 2011a)
H^{Flood}_{Dry}	Maximum water storage of the dry land	0.101	m	
kc^T_{Dry}	Crop factor of the dry land	0.5–1.4		0.38–1.42 (Liu et al., 2002)
$\lambda_{DryUGSeep}$	Exponential order for seepage in the paddy-land groundwater	1.160		
Parameters in the water management module				
$H^{Max}_{Culvert}$	Maximum water storage of the surface water controlled by the culvert	1.443	m	
$k^{Max}_{Culvert}$	Maximum water export rate through culvert	0.040	m d^{-1}	
$\lambda_{Culvert}$	Exponential order for water export through culvert	2.862		
α_{Irr}	Irrigation efficiency	0.50		
Parameters in the paddy and dry-land nitrogen module				
k_{xNOFix}	N_2 fixation rate in the dry and paddy lands	0.012	kg ha^{-1} d^{-1}	0.036 (Hofmeier et al., 2015) 0.012 (Zhao et al., 2011b)

Table A2 (*continued*)

Symbol	Parameter	Value	Unit	Values from previous references
k_{xNHNit}	Maximum nitrification rate in the dry and paddy lands	0.07	d^{-1}	0.01 (Wade et al., 2002) 0.02–2.0 (Liang et al., 2014)
$k_{xNODenit}$	Maximum denitrification rate in the dry and paddy lands	0.73	d^{-1}	
$k_{xNOUptake}$	Maximum *NO* uptake rate of crops in the dry and paddy lands	1.31/ 1.88	kg ha^{-1} d^{-1}	0.85 (Zhang et al., 2013) 0.98 (Hofmeier et al., 2015) 0.94 (Zhao et al., 2009)
$k_{xNHMine}$	Maximum mineralization rate in the dry and paddy lands	0.36	kg ha^{-1} d^{-1}	0.45 (Zhang et al., 2013) 0.2–0.46 (Zhao et al., 2011b)
$k_{xNHUptake}$	Maximum *NH* uptake rate of crops in the dry and paddy lands	0.85/ 0.52	kg ha^{-1} d^{-1}	0.85 (Zhang et al., 2013) 0.98 (Hofmeier et al., 2015) 0.94 (Zhao et al., 2009)
$k_{xNHVola}$	Maximum *NH* volatilization rate in the dry and paddy lands	0.04	d^{-1}	0.043–0.8 (Liang et al., 2014)
θ_x	Coefficient of temperature influence on the processes related to N dynamics in the dry and paddy lands	1.025		1.047 (Wade et al., 2002)
H_{Def}^{Max}	Maximum soil moisture deficit in the dry and paddy lands	130/142	mm	140 (Wade et al., 2002)
Parameters in the Water-area nitrogen module				
$k_{PondNHNit}$	Maximum nitrification rate in the surface water	0.0052	d^{-1}	0.005–0.05 (Bonnet and Wessen, 2001) 0.005–0.013 (Hamilton and Schladow, 1997)
$k_{PondNODenit}$	Maximum denitrification rate in the surface water	0.012	d^{-1}	0.005–0.05 (Bonnet and Wessen, 2001)
$k_{PondNOUptake}$	Maximum *NO* uptake rate of plants in the surface water	0.044		0.1 (Hu et al., 2006)
$k_{PondPNDecom}$	Maximum decomposition rate in the surface water	0.003	d^{-1}	0.015 (Hu et al., 2006)
$k_{PondSedRele}$	Maximum releasing rate of *NH* from sediment	0.032	d^{-1}	
$k_{PondNHUptake}$	Maximum *NH* uptake rate of plants in the surface water	0.098		0.3 (Hu et al., 2006)
$k_{PondPNResu}$	Resuspension rate of *PN* from sediment	0.005	g m^{-2} d^{-1}	
$k_{PondPNSettling}$	Settling rate of *PN* to sediment	0.008	m d^{-1}	
θ_{Pond}	Coefficient of temperature influence on the processes related to N dynamics in the surface water	0.002	$°C^{-2}$	0.004 (Arhonditsis and Brett, 2005)
KH_{DONit}	Half saturation constant of *DO* for nitrification	0.4	mg L^{-1}	0.4 (Omlin et al., 2001) 2.0 (Bonnet and Wessen, 2001) 0.1–1.0 (Wu and Xu, 2011)
KH_{NHNit}	Half saturation constant of *NH* for nitrification	0.3	mg L^{-1}	0.5 (Omlin et al., 2001) 0.1–1.0 (Wu and Xu, 2011)
$KH_{DODenit}$	Half saturation constant of *DO* for denitrification	0.2	mg L^{-1}	0.5 (Arhonditsis and Brett, 2005) 0.1 (Bonnet and Wessen, 2001)
$KH_{NODenit}$	Half saturation constant of *NO* for denitrification	0.1	mg L^{-1}	0.2 (Arhonditsis and Brett, 2005) 0.1 (Wu and Xu, 2011)
$KH_{NOUptake}$	Half saturation constant of *NO* for plant uptake	0.2	mg L^{-1}	0.2 (Hu et al., 2006)
$KH_{DODecom}$	Half saturation constant of *DO* for decomposition	0.8	mg L^{-1}	0.8 (Hu et al., 2006)
$KH_{NHUptake}$	Half saturation constant of *NH* for plant uptake	0.08	mg L^{-1}	0.2 (Hu et al., 2006)

Note: *DO*, dissolved oxygen; *NO*, nitrate/nitrite nitrogen; *NH*, ammonium nitrogen; *PN*, particulate nitrogen.

Table A3
Variables in the Nitrogen Dynamic Polder (NDP) model and their initial values for the case study in Polder Jian.

Symbol	Variable	(Initial) Value	Unit
State variables			
H_{Pond}^{T}	Water storage of the surface water	1.40	m
H_{Paddy}^{T}	Soil water storage of the paddy land	0.13	m
H_{Dry}^{T}	Soil water storage of the dry land	0.10	m
$H_{PaddyUG}^{T}$	Groundwater storage of the paddy land	0.40	m
H_{DryUG}^{T}	Groundwater storage of the dry land	0.40	m
PN_{Pond}^{T}	*PN* concentration of the surface water	0.022	mg L^{-1}
NO_{Pond}^{T}	*NO* concentration of the surface water	0.052	mg L^{-1}
NH_{Pond}^{T}	*NH* concentration of the surface water	0.052	mg L^{-1}
NO_{x}^{T}	*NO* concentration in the soil water of the dry and paddy lands	0.052	mg L^{-1}
NH_{x}^{T}	*NH* concentration in the soil water of the dry and paddy lands	0.052	mg L^{-1}
Input variables			
Lat	Latitude	31.485	°
S_{Pond}	Area of surface water	9607.16	m^2
S_{Town}	Residence area	20,385.11	m^2
S_{Paddy}	Paddy-land area	53,305.00	m^2
S_{Dry}	Dry-land area	23,096.71	m^2

(*continued on next page*)

Table A3 (*continued*)

Symbol	Variable	(Initial) Value	Unit
T^T_{Ave}	Daily average air temperature	-6–34.5	°C
T^T_{Max}	Daily maximum air temperature	−2.8–39.2	°C
T^T_{Min}	Daily minimum air temperature	−8.5–30.7	°C
T_{MaxMin}	Maximum difference of average air temperature between summer and winter	40.5	°C
T_{AveMin}	Minimum daily average air temperature during the simulation period	−6	°C
Wet^T	Daily average humidity	37–98	%
H^T_{Sun}	Daily sunshine hours	0–12.7	h
WS^T	Daily average wind speed	0.1–5.6	m s^{-1}
Pr^T	Daily precipitation	0–0.138	m d^{-1}
P^T_{Ave}	Daily mean atmospheric pressure	996.1 −1042.1	kPa
PN^T_{River}	*PN* concentration of the surrounding river	0.06–2.71	mg L^{-1}
NH^T_{River}	*NH* concentration of the surrounding river	0.34–2.71	mg L^{-1}
NO^T_{River}	*NO* concentration of the surrounding river	0.34–2.71	mg L^{-1}
V^T_{Irr}	Irrigation water amount	0–9506	m^3 d^{-1}
V^T_{Pump}	Pumping water amount	0–22232	m^3 d^{-1}
k_{DryDep}	Dry deposition rate of *TN*	0.028	kg ha^{-1} d^{-1}
NO^T_{xFert}	*NO* fertilization in the dry and paddy lands	0–0.56	kg ha^{-1} d^{-1}
NH^T_{xFert}	*NH* fertilization in the dry and paddy lands	0–2.22	kg ha^{-1} d^{-1}
PN^T_{Pr}	*PN* concentration of the rainfall water	0.25	mg L^{-1}
NH^T_{Pr}	*NH* concentration of the rainfall water	0.08	mg L^{-1}
NO^T_{Pr}	*NO* concentration of the rainfall water	1.10	mg L^{-1}
$TN_{PondSed}$	*TN* concentration of the sediment pore water	8.0	mg L^{-1}
d	Day number	1–366	
d_G	Day number of the start of the growing season	1–366	
TN_{Soil}	N content in the soil	0.10	g kg^{-1}
DO^T_{Pond}	Dissolved oxygen	4.3–11.2	mg L^{-1}
Intermediate variables			
ΔT	Time step		d
S_{Polder}	Polder area		m^2
ΔH^T_{Pond}	Water storage change of the surface water due to nature factors (precipitation, evaporation, infiltration and runoff from other areas)		m d^{-1}
ΔH^T_{Paddy}	Soil water storage change of the paddy land due to nature factors (precipitation, evapotranspiration and infiltration)		m d^{-1}
ΔH^T_{Dry}	Soil water storage change of the dry land due to nature factors (precipitation, evapotranspiration and infiltration)		m d^{-1}
H^T_{TownQ}	Runoff depth of the residential area		m d^{-1}
H^T_{PaddyQ}	Runoff depth of the paddy land		m d^{-1}
H^T_{DryQ}	Runoff depth of the dry land		m d^{-1}
$H^T_{PondPaddyUGExchange}$	Water exchange rate between paddy-land groundwater and surface water		m d^{-1}
$H^T_{PondDryUGExchange}$	Water exchange rate between dry-land groundwater and surface water		m d^{-1}
$H^T_{PaddyUGExchange}$	Water exchange rate between soil water and paddy-land groundwater		m d^{-1}
$H^T_{DryUGExchange}$	Water exchange rate between soil water and dry-land groundwater		m d^{-1}
$H^T_{PondSeep}$	Actual seepage rate of the surface water area		m d^{-1}
$H^T_{PaddyIrr}$	Soil water storage change of the paddy land due to irrigation		m d^{-1}
H^T_{Pump}	Water storage change of the surface water due to flood drainage		m d^{-1}
Pr^T_{Cum}	Accumulated precipitation in a rainfall event		m
E^T_{Pond}	Surface water evaporation		m d^{-1}
E^T_{Paddy}	Paddy-land evapotranspiration		m d^{-1}
E^T_{Dry}	Dry-land evapotranspiration		m d^{-1}
$H^T_{Culvert}$	Water storage change through the culvert		m d^{-1}
TN^T_{Pond}	*TN* concentration of the surface water		mg L^{-1}
TN^T_{River}	*TN* concentration of the surrounding river		mg L^{-1}
TN^T_{TownQ}	*TN* concentration of the residence-area runoff		mg L^{-1}
TN^T_{PaddyQ}	*TN* concentration of the paddy-land runoff		mg L^{-1}
TN^T_{DryQ}	*TN* concentration of the dry-land runoff		mg L^{-1}
ΔTN^T_{Polder}	*TN* export amount from the polder		kg
ΔTN^T_{Pump}	*TN* export amount due to flood drainage		kg
$\Delta TN^T_{Culvert}$	*TN* export amount due to culvert drainage		kg
ΔTN^T_{Seep}	*TN* export amount due to seepage		kg
ΔTN^T_{Irr}	*TN* import amount due to irrigation		kg
ΔTN^T_{Dep}	*TN* import amount due to deposition		kg
ΔNO^T_{xDep}	Mass change of *NO* in the soil water of the dry and paddy lands due to deposition		g m^{-2}
ΔNH^T_{xNit}	Mass change of *NO* in the soil water of the dry and paddy lands due to nitrification		g m^{-2}

Table A3 (*continued*)

Symbol	Variable	(Initial) Value	Unit
ΔNO^T_{xDenit}	Mass change of *NO* in the soil water of the dry and paddy lands due to denitrification		g m^{-2}
$\Delta NO^T_{xUptake}$	Mass change of *NO* in the soil water of the dry and paddy lands due to crop uptake		g m^{-2}
f_{xT}	Temperature limitation factor in the dry and paddy lands		
f_{xW}	Soil moisture limitation factor in the dry and paddy lands		
f_{xS}	Seasonal plant growth index in the dry and paddy lands		
ΔNH^T_{xDep}	Mass change of *NH* in the soil water of the dry and paddy lands due to deposition		g m^{-2}
ΔNH^T_{xMine}	Mass change of *NH* in the soil water of the dry and paddy lands due to mineralization		g m^{-2}
$\Delta NH^T_{xUptake}$	Mass change of *NH* in the soil water of the dry and paddy lands due to crop uptake		g m^{-2}
ΔNH^T_{xVola}	Mass change of *NH* in the soil water of the dry and paddy lands due to volatilization		g m^{-2}
T^T_{Soil}	Soil water temperature		°C
T^T_{Water}	Surface water temperature		°C
H_{Def}	The soil moisture deficit		m
PN_{Runoff}	*PN* concentration of the dry and paddy-land runoff		mg L^{-1}
Sed	Annual sediment yield		kg ha^{-1} yr^{-1}
R_{USLE}	Rainfall erosion factor		
K_{USLE}	Soil erodibility factor		
L_{USLE}	Topographic factor		
S_{USLE}	Coarse fragment factor		
C_{USLE}	Cover and management factor		
P_{USLE}	Support practice factor		
$\Delta NO^T_{PondDep}$	Mass change of *NO* in the surface water due to deposition		g m^{-2}
$\Delta NH^T_{PondNit}$	Concentration change of *NO* in the surface water due to nitrification		mg L^{-1}
$\Delta NO^T_{PondDenit}$	Concentration change of *NO* in the surface water due to denitrification		mg L^{-1}
$\Delta NO^T_{PondUptake}$	Concentration change of *NO* in the surface water due to plant uptake		mg L^{-1}
NO^T_{TownQ}	*NO* concentration of the residence-area runoff		mg L^{-1}
NO^T_{PaddyQ}	*NO* concentration of the paddy-land runoff		mg L^{-1}
NO^T_{DryQ}	*NO* concentration of the dry-land runoff		mg L^{-1}
$\Delta NH^T_{PondDep}$	Mass change of *NH* in the surface water due to deposition		g m^{-2}
$\Delta PN^T_{PondDecom}$	Concentration change of *NH* in the surface water due to decomposition		mg L^{-1}
$\Delta NH^T_{PondRele}$	Mass change of *NH* in the surface water due to sediment releasing		g m^{-2}
$\Delta NH^T_{PondUptake}$	Concentration change of *NH* in the surface water due to plant uptake		mg L^{-1}
NH^T_{TownQ}	*NH* concentration of the residence-area runoff		mg L^{-1}
NH^T_{PaddyQ}	*NH* concentration of the paddy-land runoff		mg L^{-1}
NH^T_{DryQ}	*NH* concentration of the dry-land runoff		mg L^{-1}
$\Delta PN^T_{PondDep}$	Mass change of *PN* in the surface water due to deposition		g m^{-2}
$\Delta PN^T_{PondResu}$	Concentration change of *PN* in the surface water due to *PN* resuspension		mg L^{-1}
$\Delta PN^T_{PondSettling}$	Concentration change of *PN* in the surface water due to *PN* settling		mg L^{-1}
PN^T_{TownQ}	*PN* concentration of the residence-area runoff		mg L^{-1}
PN^T_{PaddyQ}	*PN* concentration of the paddy-land runoff		mg L^{-1}
PN^T_{DryQ}	*PN* concentration of the dry-land runoff		mg L^{-1}
f_{PondT}	Temperature limitation factor in the surface water		
f_{DONit}	*DO* limitation factor for nitrification		
f_{NHNit}	*NH* limitation factor for nitrification		
$f_{DODenit}$	*DO* limitation factor for denitrification		
$f_{NODenit}$	*NO* limitation factor for denitrification		
$f_{NOUptake}$	*NO* limitation factor for plant uptake		
$f_{NHUptake}$	*NH* limitation factor for plant uptake		
$f_{DODecom}$	*DO* limitation factor for decomposition		
f_{Season}	Seasonal change of aquatic plant		

Note: *DO*, dissolved oxygen; *NO*, nitrate/nitrite nitrogen; *NH*, reduced nitrogen; *PN*, particulate nitrogen; *TN*, total nitrogen ($TN = NO + NH + PN$); N, nitrogen.

References

Allen, R.G., Pereira, L.S., Raes, D., Smith, M., 1998. Crop evapotranspiration-Guidelines for computing crop water requirements. Food Agric. Organ Unit. Nation. 300 (9), D05109.

Arhonditsis, G.B., Brett, M.T., 2004. Evaluation of the current state of mechanistic aquatic biogeochemical modeling. Mar. Ecol. Prog. Ser. 271, 13–26. https://doi.org/10.3354/meps271013.

Arhonditsis, G.B., Brett, M.T., 2005. Eutrophication model for Lake Washington (USA): Part I. Model description and sensitivity analysis. Ecol. Model. 187 (2–3), 140–178. https://doi.org/10.1016/j.ecolmodel.2005.01.040.

Arhonditsis, G.B., Qian, S.S., Stow, C.A., Lamon, E.C., Reckhow, K.H., 2007. Eutrophication risk assessment using Bayesian calibration of process-based models: application to a mesotrophic lake. Ecol. Model. 208 (2–4), 215–229. https://doi.org/10.1016/j.ecolmodel.2007.05.020.

Arnold, J.G., Moriasi, D.N., Gassman, P.W., Abbaspour, K.C., White, M.J., Srinivasan, R., Santhi, C., Harmel, R., Van Griensven, A., Van Liew, M.W., 2012. SWAT: model use, calibration, and validation. Trans. of the ASABE 55 (4), 1491–1508. https://doi.org/10.13031/2013.42256.

Barrett, M.E., Irish, L.B., Malina, J.F., Charbeneau, R.J., 1998. Characterization of highway runoff in Austin, Texas. Area. J. Environ. Eng. 124 (2), 131–137. https://doi.org/10.1061/(ASCE)0733-9372(1998)124:2(131).

Beven, K., 2006. A manifesto for the equifinality thesis. J. Hydrol. 320 (1), 18–36. https://doi.org/10.1016/j.jhydrol.2005.07.007.

Bonnet, M.P., Wessen, K., 2001. ELMO, a 3-D water quality model for nutrients and

chlorophyll: first application on a lacustrine ecosystem. Ecol. Model. 141 (1–3), 19–33. https://doi.org/10.1016/S0304-3800(00)00434-8.
Brauer, C.C., Torfs, P.J.J.F., Teuling, A.J., Uijlenhoet, R., 2014. The Wageningen Lowland Runoff Simulator (WALRUS): application to the hupsel brook catchment and cabauw polder. Hydrol. Earth Syst. Sci. 18 (10), 4007–4028. https://doi.org/10.5194/hessd-11-2091-2014.
Cai, J., Liu, Y., Lei, T., Pereira, L.S., 2007. Estimating reference evapotranspiration with the FAO Penman-Monteith equation using daily weather forecast messages. Agric. For. Meteorol. 145 (1–2), 22–35. https://doi.org/10.1016/j.agrformet.2007.04.012.
Cariboni, J., Gatelli, D., Liska, R., Saltelli, A., 2007. The role of sensitivity analysis in ecological modelling. Ecol. Model. 203 (1–2), 167–182. https://doi.org/10.1016/j.ecolmodel.2005.10.045.
Castelletti, A., Galelli, S., Ratto, M., Soncini-Sessa, R., Young, P.C., 2012. A general framework for Dynamic Emulation Modelling in environmental problems. Environ. Model. Software 34, 5–18. https://doi.org/10.1016/j.envsoft.2012.01.002.
Chen, D., Gao, G., Xu, C., Guo, J., Ren, G., 2005. Comparison of the Thornthwaite method and pan data with the standard Penman-Monteith estimates of reference evapotranspiration in China. Clim. Res. 28 (2), 123–132. https://doi.org/10.3354/cr028123.
Chen, S.K., Liu, C.W., 2002. Analysis of water movement in paddy rice fields (I) experimental studies. J. Hydrol. 260 (1–4), 206–215. https://doi.org/10.1016/S0022-1694(01)00615-1.
Cheng, W., Wang, C., Zhu, Y., 2006. Taihu Basin Model, first ed. HoHai University Press, Nanjing (In Chinese).
Goldberg, D., 1989. Genetic Algorithms in Search, Optimization and Machine Learning. Addison-Wesley, Boston.
Hamilton, D.P., Schladow, S.G., 1997. Prediction of water quality in lakes and reservoirs. Part I – model description. Ecol. Model. 96 (1–3), 91–110. https://doi.org/10.1016/S0304-3800(96)00062-2.
Hofmeier, M., Roelcke, M., Han, Y., Lan, T., Bergmann, H., Böhm, D., Cai, Z., Nieder, R., 2015. Nitrogen management in a rice-wheat system in the Taihu Region: recommendations based on field experiments and surveys. Agric. Ecosyst. Environ. 209, 60–73. https://doi.org/10.1016/j.agee.2015.03.032.
Hu, W., Jørgensen, S.E., Zhang, F., 2006. A vertical-compressed three-dimensional ecological model in Lake Taihu, China. Ecol. Model. 190 (3–4), 367–398. https://doi.org/10.1016/j.ecolmodel.2005.02.024.
Huang, J., Gao, J., Hörmann, G., 2012. Hydrodynamic-phytoplankton model for short-term forecasts of phytoplankton in Lake Taihu, China. Limnologica 42 (1), 7–18. https://doi.org/10.1016/j.limno.2011.06.003.
Huang, J., Gao, J., Yan, R., 2016. A Phosphorus Dynamic model for lowland Polder systems (PDP). Ecol. Eng. 88, 242–255. https://doi.org/10.1016/j.ecoleng.2015.12.033.
Kim, D.-K., Zhang, W., Hiriart-Baer, V., Wellen, C., Long, T., Boyd, D., Arhonditsis, G.B., 2014. Towards the development of integrated modelling systems in aquatic biogeochemistry: a Bayesian approach. J. Gt. Lakes Res. 40, 73–87. https://doi.org/10.1016/j.jglr.2014.04.005.
Kim, D.K., Cao, H., Jeong, K.S., Recknagel, F., Joo, G.J., 2007. Predictive function and rules for population dynamics of Microcystis aeruginosa in the regulated Nakdong River (South Korea), discovered by evolutionary algorithms. Ecol. Model. 203 (1–2), 147–156. https://doi.org/10.1016/j.ecolmodel.2006.03.040.
Kinnell, P.I.A., 2010. Event soil loss, runoff and the Universal Soil Loss Equation family of models: a review. J. Hydrol. 385 (1–4), 384–397. https://doi.org/10.1016/j.jhydrol.2010.01.024.
Krause, P., Boyle, D., Bäse, F., 2005. Comparison of different efficiency criteria for hydrological model assessment. Adv. Geosci. 5, 89–97. https://doi.org/10.5194/adgeo-5-89-2005.
Lai, G., Yu, G., Gui, F., 2006. Preliminary study on assessment of nutrient transport in the Taihu Basin based on SWAT modeling. Sci. China Series D 49 (1), 135–145. https://doi.org/10.1007/s11430-006-8113-9.
Lazar, A.N., Butterfield, D., Futter, M.N., Rankinen, K., Thouvenot-Korppoo, M., Jarritt, N., Lawrence, D.S.L., Wade, A.J., Whitehead, P.G., 2010. An assessment of the fine sediment dynamics in an upland river system: INCA-Sed modifications and implications for fisheries. Sci. Total Environ. 408 (12), 2555–2566. https://doi.org/10.1016/j.scitotenv.2010.02.030.
Legates, D.R., McCabe Jr., G.J., 1999. Evaluating the use of "goodness-of-fit" measures in hydrologic and hydroclimatic model validation. Water Resour. Res. 35 (1), 233–241. https://doi.org/10.1029/1998WR900018.
Li, Y., Šimůnek, J., Jing, L., Zhang, Z., Ni, L., 2014. Evaluation of water movement and water losses in a direct-seeded-rice field experiment using Hydrus-1D. Agric. Water Manag. 142, 38–46. https://doi.org/10.1016/j.agwat.2014.04.021.
Li, Z., Luo, C., Xi, Q., Li, H., Pan, J., Zhou, Q., Xiong, Z., 2015. Assessment of the AnnAGNPS model in simulating runoff and nutrients in a typical small watershed in the Taihu Lake basin, China. Catena 133, 349–361. https://doi.org/10.1016/j.catena.2015.06.007.
Liang, X., Chen, Y., Li, H., Tian, G., Ni, W., He, M., Zhang, Z., 2007. Modeling transport and fate of nitrogen from urea applied to a near-trench paddy field. Environ. Pollut. 150 (3), 313–320. http://doi.org/10.1016/j.envpol.2007.02.003.
Liang, X., Yuan, J., He, M., Li, H., Li, L., Tian, G., 2014. Modeling the fate of fertilizer N in paddy rice systems receiving manure and urea. Geoderma 228–229, 54–61. https://doi.org/10.1016/j.geoderma.2013.09.002.
Lindenschmidt, K.-E., Pech, I., Baborowski, M., 2009. Environmental risk of dissolved oxygen depletion of diverted flood waters in river polder systems – a quasi-2D flood modelling approach. Sci. Total Environ. 407 (5), 1598–1612. https://doi.org/10.1016/j.scitotenv.2008.11.024.
Liu, C., Zhang, X., Zhang, Y., 2002. Determination of daily evaporation and evapotranspiration of winter wheat and maize by large-scale weighing lysimeter and micro-lysimeter. Agric. For. Meteorol. 111 (2), 109–120. https://doi.org/10.1016/S0168-1923(02)00015-1.
Liu, S., Butler, D., Brazier, R., Heathwaite, L., Khu, S.-T., 2007. Using genetic algorithms to calibrate a water quality model. Sci. Total Environ. 374 (2–3), 260–272. https://doi.org/10.1016/j.scitotenv.2006.12.042.
Liu, X., Zhang, Y., Han, W., Tang, A., Shen, J., Cui, Z., Vitousek, P., Erisman, J.W., Goulding, K., Christie, P., Fangmeier, A., Zhang, F., 2013. Enhanced nitrogen deposition over China. Nature 494 (7438), 459–462. https://doi.org/10.1038/nature11917.
Neitsch, S., Arnold, J., Kiniry, J., Williams, J., King, K., 2005. SWAT theoretical documentation. Soil and Water Res. Lab. Grasslands 494, 234–235.
Omlin, M., Reichert, P., Forster, R., 2001. Biogeochemical model of Lake Züich: model equations and results. Ecol. Model. 141 (1–3), 77–103. https://doi.org/10.1016/S0304-3800(01)00256-3.
Park, R.A., Clough, J.S., Wellman, M.C., 2008. AQUATOX: modeling environmental fate and ecological effects in aquatic ecosystems. Ecol. Model. 213 (1), 1–15. https://doi.org/10.1016/j.ecolmodel.2008.01.015.
Qiao, J., Yang, L., Yan, T., Xue, F., Zhao, D., 2012. Nitrogen fertilizer reduction in rice production for two consecutive years in the Taihu Lake area. Agric. Ecosyst. Environ. 146 (1), 103–112. https://doi.org/10.1016/j.agee.2011.10.014.
Qin, B., Zhu, G., Gao, G., Zhang, Y., Li, W., Paerl, H.W., Carmichael, W.W., 2010. A drinking water crisis in Lake Taihu, China: linkage to climatic variability and lake management. Environ. Manag. 45 (1), 105–112. https://doi.org/10.1007/s00267-009-9393-6.
Reichert, P., White, G., Bayarri, M.J., Pitman, E.B., 2011. Mechanism-based emulation of dynamic simulation models: concept and application in hydrology. Comput. Stat. Data Anal. 55 (4), 1638–1655. https://doi.org/10.1016/j.csda.2010.10.011.
Richter, J., Roelcke, M., 2000. The N-cycle as determined by intensive agriculture – examples from central Europe and China. Nutr. Cycl. Agroecosyst. 57 (1), 33–46. https://doi.org/10.1023/a:1009802225307.
Rossi, L., de Alencastro, L., Kupper, T., Tarradellas, J., 2004. Urban stormwater contamination by polychlorinated biphenyls (PCBs) and its importance for urban water systems in Switzerland. Sci. Total Environ. 322 (1–3), 179–189. https://doi.org/10.1016/S0048-9697(03)00361-9.
Segeren, W.A., 1983. Introduction to polders of the world. Water Int. 8 (2), 51–54. https://doi.org/10.1080/02508068308686006.
Sophocleous, M., 2002. Interactions between groundwater and surface water: the state of the science. Hydrogeol. J. 10 (1), 52–67. https://doi.org/10.1007/s10040-001-0170-8.
Taebi, A., Droste, R.L., 2004. Pollution loads in urban runoff and sanitary wastewater. Sci. Total Environ. 327 (1–3), 175–184. https://doi.org/10.1016/j.scitotenv.2003.11.015.
Tetra Tech, I., 2007. The Environmental Fluid Dynamics Code: Theory and Computation. US EPA, Fairfax, VA.
van der Grift, B., Broers, H.P., Berendrecht, W., Rozemeijer, J., Osté, L., Griffioen, J., 2016. High-frequency monitoring reveals nutrient sources and transport processes in an agriculture-dominated lowland water system. Hydrol. Earth Syst. Sci. 20 (5), 1851–1868. https://doi.org/10.5194/hess-20-1851-2016.
Wade, A., Durand, P., Beaujouan, V., Wessel, W., Raat, K., Whitehead, P., Butterfield, D., Rankinen, K., Lepisto, A., 2002. A nitrogen model for European catchments: INCA, new model structure and equations. Hydrol. Earth Syst. Sci. 6 (3), 559–582. https://doi.org/10.5194/hess-6-559-2002.
Wade, A.J., Butterfield, D., Whitehead, P.G., 2006. Towards an improved understanding of the nitrate dynamics in lowland, permeable river-systems: applications of INCA-N. J. Hydrol. 330 (1–2), 185–203. https://doi.org/10.1016/j.jhydrol.2006.04.023.
Wang, S., Shan, J., Xia, Y., Tang, Q., Xia, L., Lin, J., Yan, X., 2017. Different effects of biochar and a nitrification inhibitor application on paddy soil denitrification: a field experiment over two consecutive rice-growing seasons. Sci. Total Environ. 593–594, 347–356. http://doi.org/10.1016/j.scitotenv.2017.03.159.
Wellen, C., Kamran-Disfani, A.-R., Arhonditsis, G.B., 2015. Evaluation of the current state of distributed watershed nutrient water quality modeling. Environ. Sci. Technol. 49 (6), 3278–3290. https://doi.org/10.1021/es5049557.
Whitehead, P.G., Leckie, H., Rankinen, K., Butterfield, D., Futter, M.N., Bussi, G., 2016. An INCA model for pathogens in rivers and catchments: model structure, sensitivity analysis and application to the River Thames catchment, UK. Sci. Total Environ. 572, 1601–1610. https://doi.org/10.1016/j.scitotenv.2016.01.128.
Wu, G., Xu, Z., 2011. Prediction of algal blooming using EFDC model: case study in the Daoxiang Lake. Ecol. Model. 222 (6), 1245–1252. https://doi.org/10.1016/j.ecolmodel.2010.12.021.
Xu, J., Peng, S., Yang, S., Wang, W., 2012. Ammonia volatilization losses from a rice paddy with different irrigation and nitrogen managements. Agric. Water Manag. 104, 184–192. http://doi.org/10.1016/j.agwat.2011.12.013.
Yan, R., Gao, J., Huang, J., 2016. WALRUS-paddy model for simulating the hydrological processes of lowland polders with paddy fields and pumping stations. Agric. Water Manag. 169, 148–161. https://doi.org/10.1016/j.agwat.2016.02.018.
Young, R.A., Onstad, C., Bosch, D., Anderson, W., 1989. AGNPS: a nonpoint-source pollution model for evaluating agricultural watersheds. J. Soil Water Conserv. 44 (2), 168–173.
Zhang, J.-H., Liu, J.-L., Zhang, J.-B., Cheng, Y.-N., Wang, W.-P., 2013. Nitrate-nitrogen dynamics and nitrogen budgets in rice-wheat rotations in Taihu lake region, China. Pedosphere 23 (1), 59–69. https://doi.org/10.1016/S1002-0160(12)60080-0.

Zhao, G., Hörmann, G., Fohrer, N., Gao, J., Li, H., Tian, P., 2011a. Application of a simple raster-based hydrological model for streamflow prediction in a humid catchment with polder systems. Water Resour. Manag. 25 (2), 661–676. https://doi.org/10.1007/s11269-010-9719-4.

Zhao, G., Hörmann, G., Fohrer, N., Li, H., Gao, J., Tian, K., 2011b. Development and application of a nitrogen simulation model in a data scarce catchment in South China. Agric. Water Manag. 98 (4), 619–631. https://doi.org/10.1016/j.agwat.2010.10.022.

Zhao, X., Xie, Y., Xiong, Z., Yan, X., Xing, G., Zhu, Z., 2009. Nitrogen fate and environmental consequence in paddy soil under rice-wheat rotation in the Taihu lake region, China. Plant Soil 319 (1), 225–234. https://doi.org/10.1007/s11104-008-9865-0.

Zhao, X., Zhou, Y., Wang, S., Xing, G., Shi, W., Xu, R., Zhu, Z., 2012. Nitrogen balance in a highly fertilized rice–wheat double-cropping system in southern China. Soil Sci. Soc. Am. J. 76 (3), 1068–1078. https://doi.org/10.2136/sssaj2011.0236.

TOWARDS THE DEVELOPMENT OF A MODELING FRAMEWORK TO TRACK NITROGEN EXPORT FROM LOWLAND ARTIFICIAL WATERSHEDS (POLDERS)

SUPPORTING INFORMATION

Jiacong Huang[a,b], George B. Arhonditsis[b], Junfeng Gao[a*], Dong-Kyun Kim[b], Feifei Dong[b]

[a]*Key Laboratory of Watershed Geographic Sciences, Nanjing Institute of Geography and Limnology, Chinese Academy of Sciences, 73 East Beijing Road, Nanjing 210008, China*

[b]*Ecological Modelling Laboratory, Department of Physical & Environmental Sciences, University of Toronto, Toronto, ON M1C 1A4, Canada*

* Corresponding author. Tel & Fax: +86-25-86882124; E-mail address: gaojunf@niglas.ac.cn

1. Water exchange between polder systems and surrounding rivers

Water exchange between polder systems and surrounding rivers differs from freely draining catchments, in the sense that it is predominantly controlled by anthropogenic interventions. The manual control of water included the processes of agricultural irrigation, flood and culvert drainage. To describe these processes, four threshold water levels, as well as a culvert to control the water exchange between the polder system and its surrounding rivers, were included in the water management module (Fig. SI-1). As a typical water management practice in polder systems, the culvert is closed without any water exchange during the rice season, because the rice land required a relatively high water level. On the other hand, the farmland does not require high water levels during the non-rice season, and therefore the culvert is open for water export from the polder system to its surrounding rivers.

During the rice season, an irrigation event would occur when the water level is as low as $H_{Pond}^{StartIrr}$ (or threshold water level to start irrigation pump), and would stop when the water level increased to $H_{Pond}^{StopIrr}$ (or threshold water level to stop irrigation pump). During the flood period, the water level of the polder system is lower than its surrounding rivers. The pump would export the water out of the polder system when the water level is as high as $H_{Pond}^{StartExport}$ (or threshold water level to start flood pump), and would stop when the water level decreased to $H_{Pond}^{StopExport}$ (or threshold water level to stop flood pump).

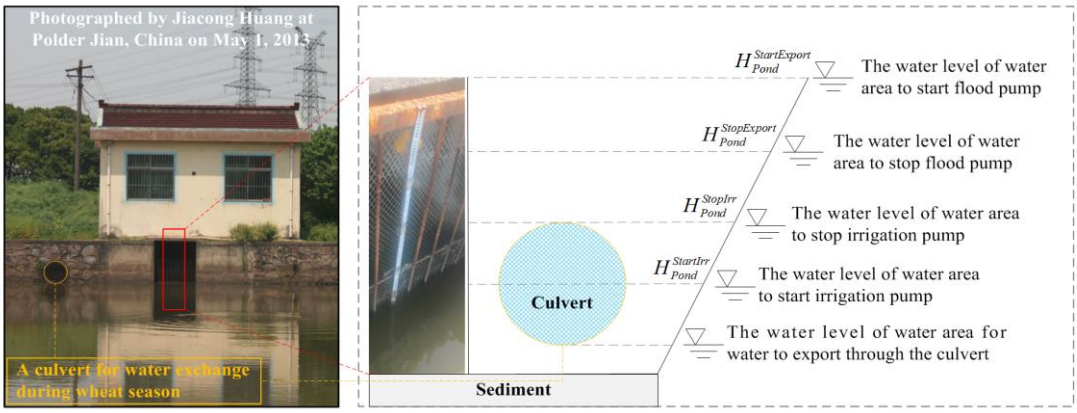

Fig. SI-1: Threshold water levels used to control water exchange between the polder and its surrounding rivers

2. Empirical relationship between water temperature and air temperature

Surface water temperature (T_{Water}^{T} in Equation 6.10) was calculated based on air temperature. Their relationship was estimated based on measured water and air temperatures during the period between Feb. 1 and Dec. 31, 2016 (Fig. SI-2).

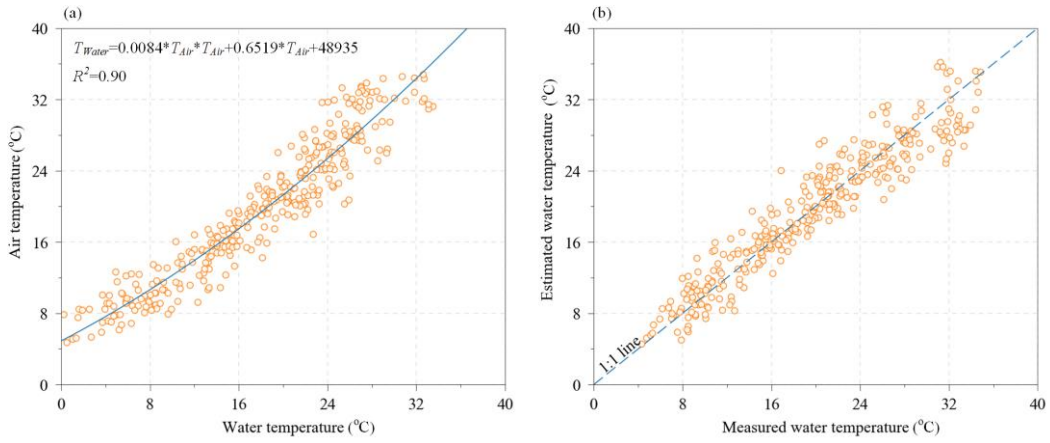

Fig. SI-2: (a) The fitted curve between air temperature and water temperature; **(b)** Measured and estimated temperature in surface water. T_{Water}, water temperature (°C); T_{Air}, air temperature (°C).

3. Sensitivity analysis results

Based on our sensitivity analysis exercise, the top ten most influential parameters in the water balance and nitrogen (N) dynamic modules of the Nitrogen Dynamic Polder (NDP) model are provided in Table SI-1, where we also present their ranges along with their initial values and those assigned after optimization (calibrated values).

Table SI-1: Value range and sensitivity value of the parameters in the Nitrogen Dynamic Polder (NDP) model.

Symbol	Parameter	Sensitivity value	Value range	Initial value	Calibrated value
Parameters in the water-area water balance module					
α_{Ev}	Ratio between reference evapotranspiration and surface water evaporation	0.002	0.4-0.8	0.572	0.572
$k_{PondSeepMax}$	Maximum seepage rate of the surface water area (m d^{-1})	0.035	0-0.01	0.001	0.0004
$\lambda_{PondSeep}$	Exponential order for seepage in the surface water area	0.016	0-2.0	0.20	0.17
$\lambda_{Pond2DryUG}$	Exponential order for water transport from surface water to dry-land groundwater	0.016	0-2.0	0.10	0.013
$\lambda_{DryUG2Pond}$	Exponential order for water transport from dry-land groundwater to surface water	0.013	0-2.0	0.12	0.085
$\lambda_{Pond2PaddyUG}$	Exponential order for water transport from surface water to paddy-land groundwater	0.042	0-2.0	0.25	0.218
$\lambda_{PaddyUG2Pond}$	Exponential order for water transport from paddy-land groundwater to surface water	0.015	0-2.0	0.74	0.624
Parameters in the residential-area water balance module					
rc_{Town}	Runoff coefficient for the residential area	0.001	0.55-0.75	0.685	0.685
$H_{TownFill}$	Water fill amount of the residential area (m)	0.004	0.002-0.01	0.002	0.002
Parameters in the paddy-land water balance module					
$k_{PaddyInfMax}$	Maximum infiltration rate of the paddy land (m d^{-1})	0.004	0.003-0.007	0.005	0.005

$k_{PaddyCapMax}$	Maximum capillary rise rate of the paddy land (m d^{-1})	0.001	0.003-0.007	0.006	0.006
H_{Paddy}^{Sat}	Saturated soil water of the paddy land (m)	0.001	0.08-0.17	0.120	0.120
H_{Paddy}^{Flood}	Maximum water storage of the paddy land (m)	0.005	0.15-0.17	0.158	0.158
$H_{PaddyMax}^{T}$	Upper limit of appropriate water storage for the paddy land (m)	0.005	0.12-0.17	0.13-0.17	0.13-0.17
$H_{PaddyMin}^{T}$	Lower limit of appropriate water storage for the paddy land (m)	0.005	0.10-0.12	0.10-0.11	0.10-0.11
kc_{Paddy}^{T}	Crop factor of the paddy land	0.004	0.38-1.5	0.5-1.4	0.5-1.4
$k_{UGSeepMax}$	Maximum seepage rate of the paddy and dry-land groundwater (m d^{-1})	0.028	0-0.01	0.006	0.0088
$\lambda_{PaddyUGSeep}$	Exponential order for seepage in the paddy-land groundwater	0.001	1-3	2.989	2.989
Parameters in the dry-land water balance module					
$k_{DryInfMax}$	Maximum infiltration rate of the dry land (m d^{-1})	0.002	0.003-0.007	0.003	0.003
$k_{DryCapMax}$	Maximum capillary rise rate of the dry land (m d^{-1})	0.001	0.001-0.005	0.004	0.004
H_{Dry}^{Sat}	Saturated soil water of the dry land (m)	0.001	0.08-0.17	0.088	0.088
H_{Dry}^{Flood}	Maximum water storage of the dry land (m)	0.001	0.10-0.11	0.101	0.101

kc_{Dry}^{T}	Crop factor of the dry land	0.002	0.38-1.42	0.5-1.4	0.5-1.4
$\lambda_{DryUGSeep}$	Exponential order for seepage in the paddy-land groundwater	0.002	1-3	1.160	1.160
Parameters in the water management module					
$H_{Culvert}^{Max}$	Maximum water storage of the surface water controlled by the culvert (m)	0.037	1.3-1.5	1.46	1.443
$k_{Culvert}^{Max}$	Maximum water export rate through culvert (m d^{-1})	0.040	0.01-0.04	0.03	0.040
$\lambda_{Culvert}$	Exponential order for water export through culvert	0.006	1-3	2.78	2.862
α_{Irr}	Irrigation efficiency	0.002	0-0.50	0.50	0.50
Parameters in the paddy and dry-land nitrogen module					
k_{xNOFix}	N_2 fixation rate in the dry and paddy lands (kg ha^{-1} d^{-1})	0.000	0.012-0.036	0.012	0.012
k_{xNHNit}	Maximum nitrification rate in the dry and paddy lands (d^{-1})	0.221	0.02-0.1	0.08	0.07
$k_{xNODenit}$	Maximum denitrification rate in the dry and paddy lands (d^{-1})	0.002	0-0.8	0.73	0.73
$k_{xNOUptake}$	Maximum *NO* uptake rate of crops in the dry and paddy lands (kg ha^{-1} d^{-1})	0.000/0.001	0.5-2	1.31/1.88	1.31/1.88
$k_{xNHMine}$	Maximum mineralization rate in the dry and paddy lands (kg ha^{-1} d^{-1})	0.002	0.2-0.46	0.36	0.36
$k_{xNHUptake}$	Maximum *NH* uptake rate of crops in the dry and paddy lands (kg ha^{-1} d^{-1})	0.069/0.159	0.5-2	0.82/0.42	0.86/0.52

$k_{xNHVola}$	Maximum *NH* volatilization rate in the dry and paddy lands (d^{-1})	0.001	0.043-0.8	0.04	0.04
θ_x	Coefficient of temperature influence on the processes related to N dynamics in the dry and paddy lands	0.283	1.0-1.1	1.030	1.025
H_{Def}^{Max}	Maximum soil moisture deficit in the dry and paddy lands (mm)	0.000/0.000	130-150	130/142	130/142
Parameters in the Water-area nitrogen module					
$k_{PondNHNit}$	Maximum nitrification rate in the surface water (d^{-1})	0.378	0-0.05	0.005	0.0052
$k_{PondNODenit}$	Maximum denitrification rate in the surface water (d^{-1})	0.003	0-0.05	0.012	0.012
$k_{PondNOUptake}$	Maximum *NO* uptake rate of plants in the surface water	0.048	0-0.05	0.042	0.044
$k_{PondPNDecom}$	Maximum decomposition rate in the surface water (d^{-1})	0.023	0-0.02	0.003	0.003
$k_{PondSedRele}$	Maximum releasing rate of *NH* from sediment (d^{-1})	0.732	0-0.1	0.030	0.032
$k_{PondNHUptake}$	Maximum *NH* uptake rate of plants in the surface water	0.657	0-0.1	0.090	0.098
$k_{PondPNResu}$	Resuspension rate of *PN* from sediment ($g\ m^{-2}\ d^{-1}$)	0.035	0-0.01	0.005	0.005
$k_{PondPNSettling}$	Settling rate of *PN* to sediment ($m\ d^{-1}$)	0.466	0-0.125	0.007	0.008
θ_{Pond}	Coefficient of temperature influence on the processes related to N dynamics in the surface water ($°C^{-2}$)	0.037	0-0.01	0.002	0.002

KH_{DONit}	Half saturation constant of *DO* for nitrification (mg L^{-1})	0.016	0.1-2.0	0.4	0.4
KH_{NHNit}	Half saturation constant of *NH* for nitrification (mg L^{-1})	0.025	0.1-1.0	0.3	0.3
$KH_{DODenit}$	Half saturation constant of *DO* for denitrification (mg L^{-1})	0.001	0.1-0.5	0.2	0.2
$KH_{NODenit}$	Half saturation constant of *NO* for denitrification (mg L^{-1})	0.001	0.1-0.5	0.1	0.1
$KH_{NOUptake}$	Half saturation constant of *NO* for plant uptake (mg L^{-1})	0.011	0-0.5	0.2	0.2
$KH_{DODecom}$	Half saturation constant of *DO* for decomposition (mg L^{-1})	0.001	0-1.0	0.8	0.8
$KH_{NHUptake}$	Half saturation constant of *NH* for plant uptake (mg L^{-1})	0.088	0-0.3	0.09	0.08

Note: *DO*, dissolved oxygen; *NO*, oxidized nitrogen; *NH*, reduced nitrogen; *PN*, particulate nitrogen. Ten most sensitive parameters for the water balance and nitrogen dynamic modules have grey background.

4. Parameter optimization results using a Genetic Algorithm (GA)

During the 100 generations of parameter optimization using a Genetic Algorithm, the model fit for water level and nitrogen modules was gradually improved with average fitness value (Equation 2) increasing from 1.44/0.94 (1st generation) to 1.48/1.09 (100th generation) (Fig. SI-3). The fitness range of 100 best individuals was also reduced with a standard deviation decreasing from 0.014 to 0.004. A careful inspection of Fig. SI-3 also reveals that the model fit did not improve dramatically from the 1st to 100th generation of GA. The latter pattern suggests that there are many locally optimal solutions for NDP, which is similar with the behaviour reported for other complex overparameterized models.

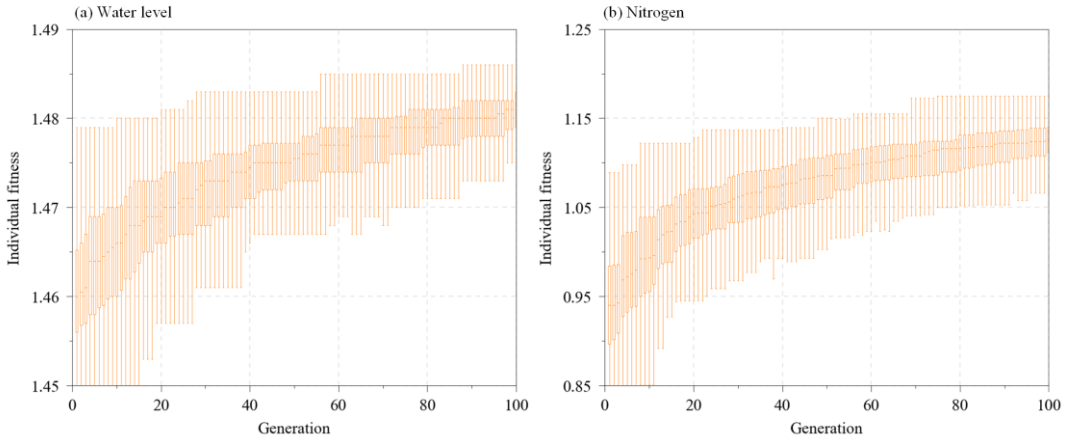

Fig. SI-3: Individual evolution over the 100 generation of parameter optimization using a Genetic Algorithm. The graph presents the 100 fitness value from the best individual of each repeated run.

5. Uncertainty analysis

5.1. Model uncertainty on key N sources and sinks

The N balance analysis (Section 3.5) revealed that the key N sources and sinks in Polder Jian were fertilization, mineralization, crop uptake, volatilization, and denitrification. In order to investigate the relative importance of the uncertainty underlying these factors on N export, we conducted a simple uncertainty analysis based on a two-step Monte Carlo simulation procedure:

- **Step 1**. Generate 1000 samples (simulations) based on random perturbations of fundamental processes of N dynamics (fertilization, mineralization, crop uptake, volatilization, and denitrification). Each sample represented random perturbations of these five processes simultaneously within a ± 10% range relative to the values assigned after model optimization.
- **Step 2**. Run all these 1000 simulations and calculate the resulting annual N export.

Our uncertainty analysis results suggested that the uncertainty associated with the fertilization and crop uptake rates is responsible for considerable variability of the annual N export. Increasing use of *NO*/*NH* fertilizer resulted in a higher (nearly linear increase) N export (Fig. SI-4a). Likewise, increasing *NO/NH* uptake rates from crops resulted in a lower N export (Fig. SI-4e). This finding implies that accurate estimates of the amount of *NO*/*NH* fertilizers implemented on annual basis (NO^{T}_{xFert} and NH^{T}_{xFert}), as well as the maximum *NO/NH* uptake rates from crops ($k_{xNOUptake}$ and $k_{xNHUptake}$) are critical in reducing model uncertainty.

Random perturbations of mineralization, volatilization, and denitrification resulted in negligible variations of annual N export (Fig. SI-4b-d), implying that a ±10% uncertainty relative to the optimal values assigned to the three parameters characterizing mineralization, volatilization, and denitrification, i.e., $k_{xNHMine}$ (maximum mineralization rate in the dry and paddy lands), $k_{xNHVola}$ (maximum NH volatilization rate in the dry and paddy lands), $k_{xNODenit}$ (maximum denitrification rate in the dry and paddy lands), may not have profound implications for the derived N export fluxes.

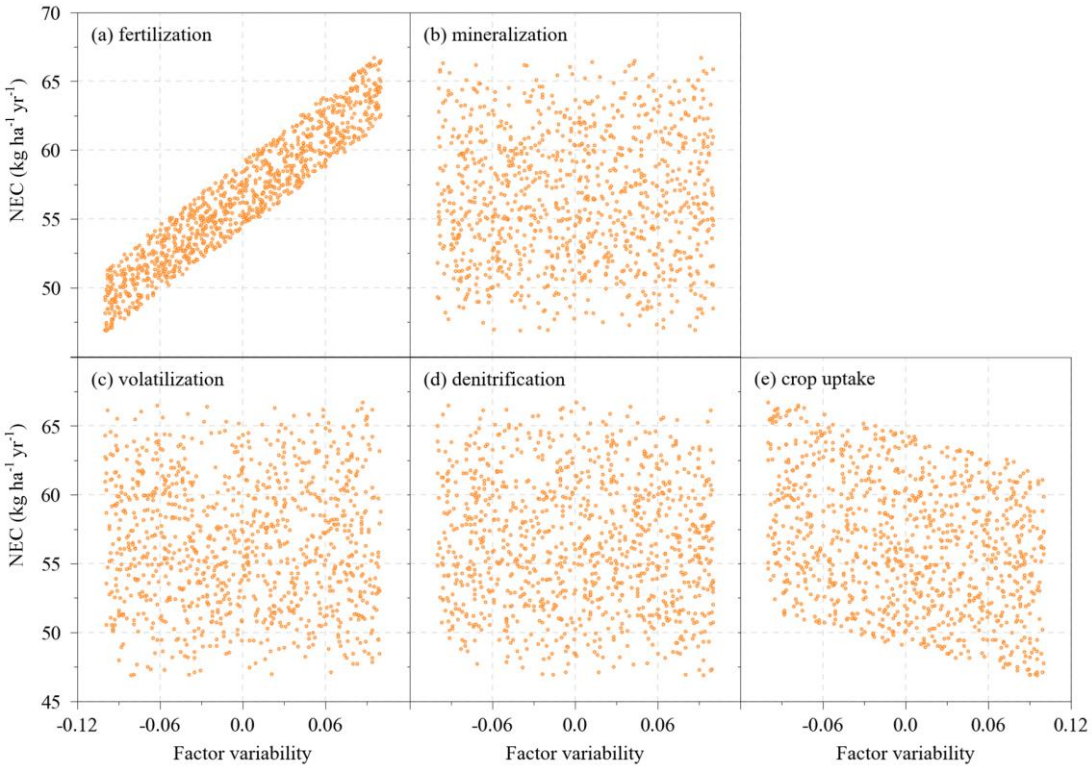

Fig. SI-4: NEC levels (N export coefficient, kg ha^{-1} yr^{-1}) driven by the uncertainty associated with fertilization (a), mineralization (b), volatilization (c), denitrification (d) and crop uptake (e). The examination of the impact of uncertainty was based on the generation of 1000 samples of the five factors collected from their ± 10% range relative to the values assigned after model optimization.

5.2. Uncertainties from parameters

The uncertainties from model parameters were investigated using a two-step Monte Carlo simulation procedure similar to that described in Section 5.1.

- **Step 1.** Generate 1000 samples based on random perturbations of twenty most influential parameters, i.e., the ten most sensitive parameters for the water balance and nitrogen dynamic modules (Table SI-1). Each sample represented random perturbations of these parameters within the ± 10% range relative to the values assigned during model optimization.
- **Step 2.** Run all these 1000 simulations and calculate the corresponding *F* values.

The scatter plots (*F* versus parameter values) for these twenty influential parameters represent proxies of the marginal parameter distributions. As shown in Fig. SI-5h, the model was more likely to achieve a high model fit with $H_{Culvert}^{Max}$ (maximum water storage of the surface water controlled by the culvert, m) values lower than 1.143. The maximum water export rate through culvert (m d^{-1}), $k_{Culvert}^{Max}$, and the coefficient of temperature influence on the processes related to N dynamics in the dry and paddy lands, θ_x, displayed a unimodal pattern (Fig. SI-5i and n). Their average values were very close to their calibrated values, 0.04 and 1.025, respectively (Table SI-1. The uninformative patterns for the rest 17 marginal distributions (Fig. SI-5) are suggestive of an interplay among the multiple parameters, characterized by distinctly different parameter combinations that provide a similar model fit. This finding is consistent with the conclusion drawn from the parameter optimization exercise (Section 4; see also Fig. SI-3).

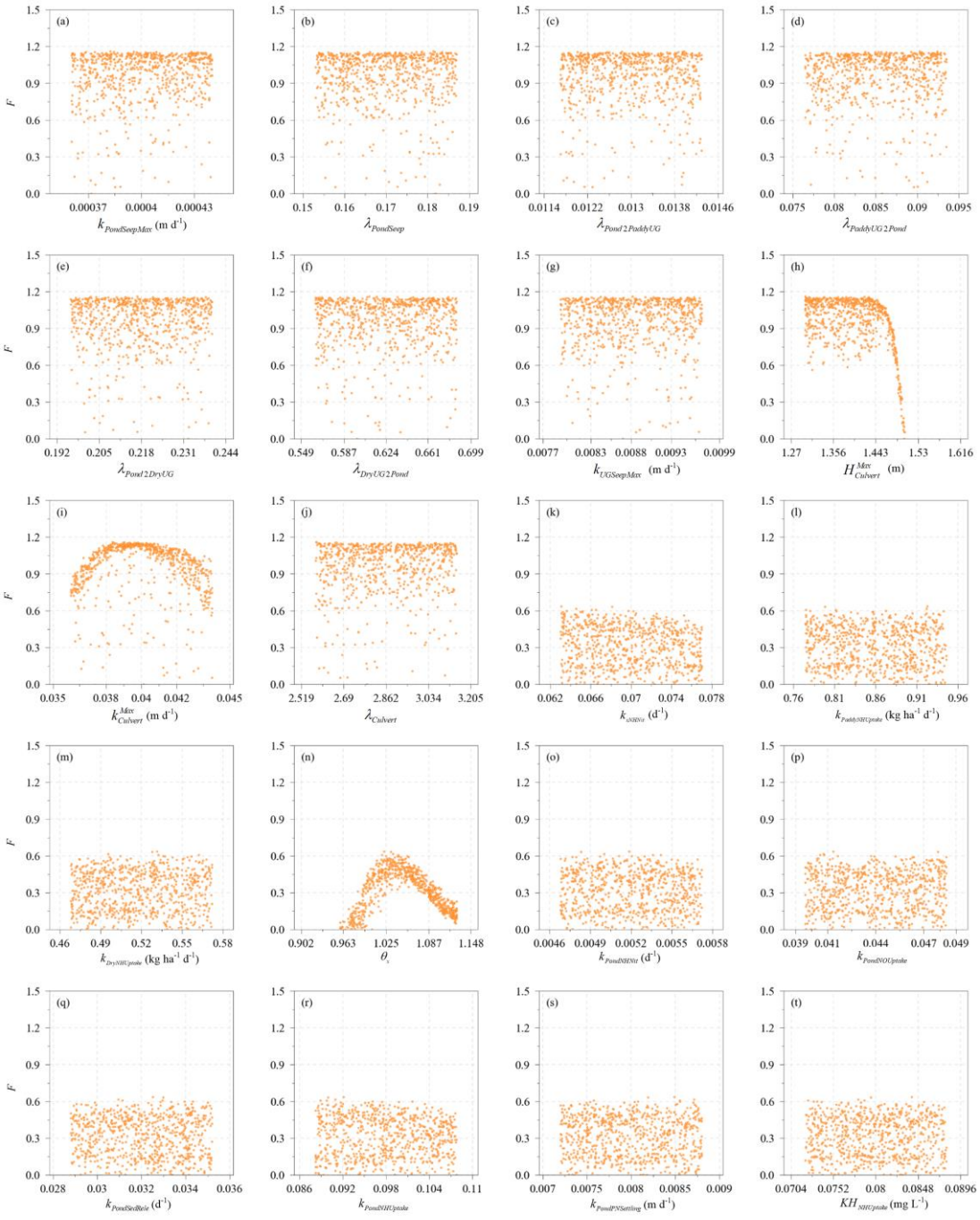

Fig. SI-5: Parameter values versus model fitness (*F*) for total nitrogen (*TN*) during the 2014-2017 period based on 1000 Monte Carlo samples of the twenty most sensitive parameters, i.e., ten sensitive parameters for the water balance and nitrogen dynamic modules, respectively. Parameter symbols can be found in Table SI-1.

The 1000 simulations also delineate a relatively large width of the 90% uncertainty zone (Fig. SI-6). It is also interesting to note that several measured *TN* concentration were still not captured by the uncertainty bounds, indicative of a more systematic

error probably stemming from model structural deficiencies or (most likely) bias introduced by model inputs or forcing functions.

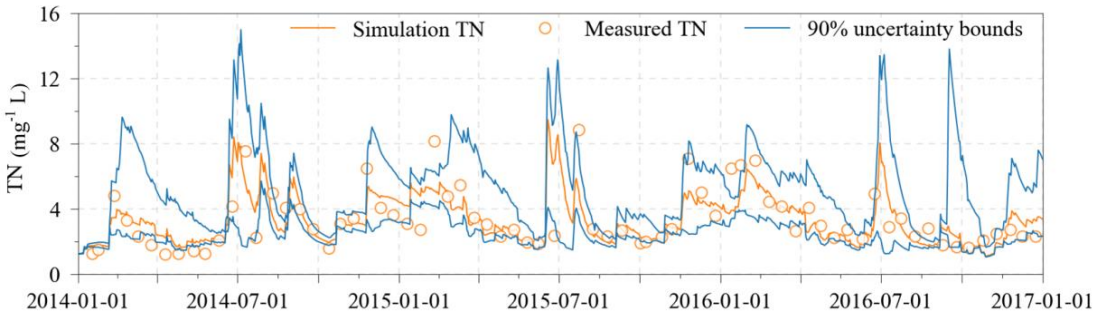

Fig. SI-6: Measured versus simulated *TN* concentrations along with the 90% uncertainty bounds (blue lines). The uncertainty zone was obtained by 1000 Monte Carlo samples of the twenty most sensitive parameters. The latter samples were collected from their ± 10% range relative to the values assigned after model optimization.

6. Model fitness function

In this study, the model fitness to evaluate model performance was based on the sum of the coefficient of determination (R^2) and Nash-Sutcliffe efficiency (*NS*) rather than solely R^2 or *NS*. Figure SI-7 shows that *F* is indeed better in describing model fit as the two metrics are characterized by a unimodal pattern. Simply put, many individual simulations (or parameter vectors) displayed high R^2 values but low *NS* values and vice versa. Thus, the use of both measures of fit offers a superior goal function to guide our optimization exercise.

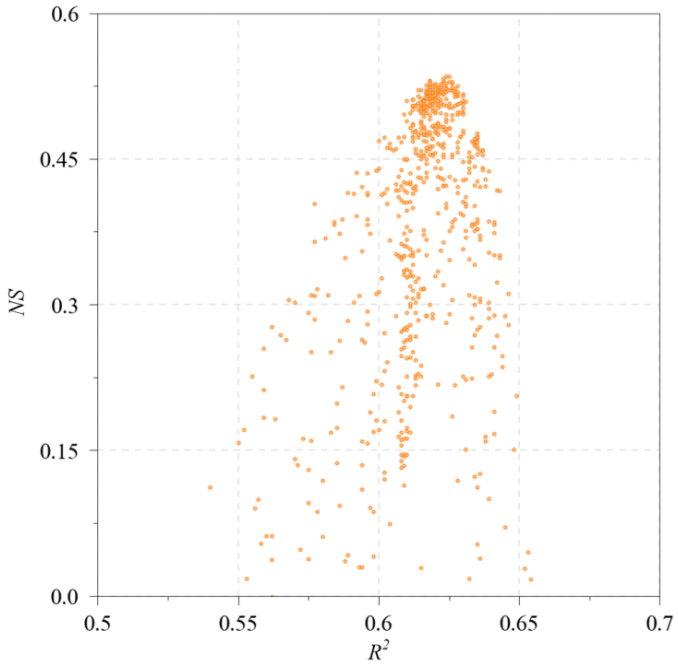

Fig. SI-7: Coefficient of determination (R^2) versus Nash-Sutcliffe efficiency (*NS*) for the water levels during the 2015-2016 period, based on the Monte Carlo analysis presented in Figures SI-5 & 6.

7. Model implementation and availability

NDP was developed as a joint endeavor with other contributors including water managers and local farmers. Water managers provided their experience on manual operations of irrigation, flood and culvert drainage for polder systems, which were not adequately described in previous literature. Agricultural regulations for describing water and N dynamics in NDP were provided by local farmers residing in Polder Jian, China.

The coding and integration work of NDP were implemented using the programming language of Python. The model can be freely used by researchers, managers, and other stakeholders. The software package for running NDP, as well as its manual and data collected from Polder Jian, China, can be downloaded freely from http://www.escience.cn/people/elake/index.html. Further information can be obtained by contacting Jiacong Huang (jchuang@niglas.ac.cn).